



4D reconstruction of the Doldenhorn nappe-basement system in the Aar massif: Insights into late-stage continent-continent collision in the Swiss Alps

Ferdinando Musso Piantelli ^{a,*}, David Mair ^a, Alfons Berger ^a, Fritz Schlunegger ^a, Michael Wiederkehr ^b, Eva Kurmann ^b, Roland Baumberger ^b, Andreas Möri ^b, Marco Herwegh ^a

^a Institute of Geological Sciences University of Bern, Baltzerstrasse 1+3, 3012 Bern, Switzerland

^b Swiss Geological Survey, Federal Office of Topography swisstopo, Seftigenstrasse 264, 3084 Bern, Switzerland

ARTICLE INFO

Keywords:

3D geological modelling
Passive margin inversion
Cross-section restoration
4D reconstruction
Fold-and-thrust belts
Alpine tectonic inversion

ABSTRACT

The inversion of passive margins and their transportation into fold-and-thrust belts is a critical stage of mountain-building processes. In this study, we selected the Doldenhorn Nappe and Aar/Gastern Massifs (Central Swiss Alps) system as an ideal laboratory to document the impact of inherited structures, their along-strike variations, and basement tectonics on the evolution of a fold-and-thrust belt. Three-dimensional geological modelling and cross-section restoration allowed us to reconstruct the 4D evolution of the investigated area during the late-stage Alpine orogeny (30 to 0 Ma). Our results demonstrate that: (i) the Doldenhorn Nappe is the product of the inversion of an asymmetric half-graben basin; (ii) variations in incipient basin sediment thicknesses correlate directly with the along-strike variation of the deformation of the Doldenhorn Nappe; and (iii) the multiphase thick-skinned deformation that overprinted the Doldenhorn Nappe from 22 Ma until today changed the shape of the Doldenhorn Nappe and Aar/Gastern Massifs. This reconstruction shows how thin-skinned nappe formation mechanisms and the nappe geometries are controlled by the initial basement geometry and by the rheological strength contrasts between basement and cover sediments. Basement-involved uplift and shortening controls then the late-stage collisional 3D overprint and mechanics of the fold-and-thrust belts.

1. Introduction

Fold-and-thrust belts are an essential component in the mid- to upper crustal deformation of most orogenic systems. Recognition of the controlling factors on their evolution is fundamental for understanding the long- and short-term dynamics of mountain building processes (e.g. Cooper, 2007; Lacombe and Bellahsen, 2016; Bigi et al., 2018; Ghani et al., 2018). Using analogue, field and numerical studies researchers have attempted for several decades to disclose the process of mechanical deformation controlling the evolution of fold-and-thrust belts (e.g. Chamberlin, 1919; Rodgers, 1949; Bally et al., 1966; Macedo and Marshak, 1999; Pfiffner, 2006; Bauville and Schmalholz, 2015, 2017; Lacombe and Bellahsen, 2016; Granado and Ruh, 2019). Quite often, however, related approaches have been restricted to two-dimensional sections neglecting the three-dimensional and often non-cylindrical architecture of fold-and-thrust belts. With the evolving capabilities in 3D modelling software and the increase in computational power, recent

studies included observations regarding the along-strike 3D variability of these systems (e.g. Macedo and Marshak, 1999; McClay et al., 2004; Sala et al., 2014; Santolaria et al., 2015; von Tscharnar et al., 2016; Ghani et al., 2018; Balestra et al., 2019). Such 3D considerations are of high relevance for an improved understanding of the evolution of fold-and-thrust belts and mountain chains in general. However, the 3D structural complexity of these systems that frequently record the result of a large range of tectonic processes renders the parameters that control the evolution of fold-and-thrust belts elusive to detect, and therefore they are still poorly understood. Hence, a single cross-sectional view of a fold-and-thrust belt does not allow resolving their entire complexity (e.g. Watts et al., 1995; Allmendinger et al., 1997; Mouthereau et al., 2002; Hamilton, 1988; Nemcok et al., 2013). The use of three-dimensional modelling and restoration techniques is thus a crucial and necessary step for characterizing the structural disposition of a fold-and-thrust belt, including reconstructing the fault network and detecting inconsistencies in structural interpretations (e.g. Turrini et al., 2014;

* Corresponding author.

E-mail address: ferdinando.musso@geo.unibe.ch (F. Musso Piantelli).

<https://doi.org/10.1016/j.tecto.2022.229586>

Received 14 February 2022; Received in revised form 9 September 2022; Accepted 11 September 2022

Available online 4 October 2022

0040-1951/© 2022 The Authors. Published by Elsevier B.V. This is an open access article under the CC BY license (<http://creativecommons.org/licenses/by/4.0/>).

Balestra et al., 2019).

It is documented that in several fold-and-thrust belts around the world (e.g. Taiwan, Himalaya) the pre-collisional geometries have controlled the kinematics of the subsequent collisional processes (Mouthereau et al., 2002; Butler et al., 2006; Zanchi et al., 2006; Bellahsen et al., 2014; Ghani et al., 2018; Curzi et al., 2020). For example, the 3-D architecture of the involved former passive continental margins, consisting of a combination of discontinuous fault systems and geometrical asymmetries, form local basins and topographic highs that can lead to extreme along-strike variations (Lacombe et al., 2003; Turini et al., 2016; Lymer et al., 2019). These variations primarily affect the shape and topography of the basins' basement and in consequence also the resulting sedimentary thicknesses, whereby basins may taper gradually or terminate with abrupt steps on their margins (Taylor et al., 1995; Mouthereau et al., 2002; Spitz et al., 2020; Vitale and Giacria, 2021; Tavani et al., 2021). Such structures can control the architecture of the developing fold-and-thrust belt when these systems are inverted and incorporated into an orogenic wedge during collision, (e.g. Gillcrist et al., 1987; Letouzey et al., 1990; Doglioni, 1992; Macedo and Marshak, 1999; Mohn et al., 2011; Boutoux et al., 2014; Mohn et al., 2014). This results in considerable differences across belts as well as along strike

variability within individual belts (Lacombe and Mouthereau, 2002; Fitz-Diaz et al., 2011; Ghani et al., 2018).

In this work, we selected the Doldenhorn Nappe (Central Swiss Alps) to document the 3D complexity of a fold-and-thrust belt. The large amount of structural (Burkhard, 1988; Hänni and Pfiffner, 2001; Herwegh and Pfiffner, 2005; Krayenbuhl and Steck, 2009; Pfiffner, 2015; Cardello and Mancktelow, 2015; Cardello and Mancktelow, 2015; Mair et al., 2018), petrologic-geochemical (Frey et al., 1980; Frey, 1987; Arkai et al., 2002; Berger et al., 2020; Girault et al., 2020) and numerical studies (Bauville and Schmalholz, 2015; von Tscharner et al., 2016; Granado and Ruh, 2019; Spitz et al., 2020) make the Doldenhorn Nappe an excellent example for documenting the impact of inherited structures and along-strike variations on the evolution of a fold-and-thrust belt. Hence, we built a 4D geological reconstruction of the Doldenhorn Nappe during the late-stage Alpine evolution (30 to 0 Ma) to examine how inherited structures and along-strike variations influenced the structural development of the nappe. In particular, we illustrate how the 3D morphology and variability of former passive continental margin conditions the mechanism and style of basin inversion during the continent-continent collision, and how this is recorded by the along-strike variations in the tectonic architecture. We thus consider the Doldenhorn

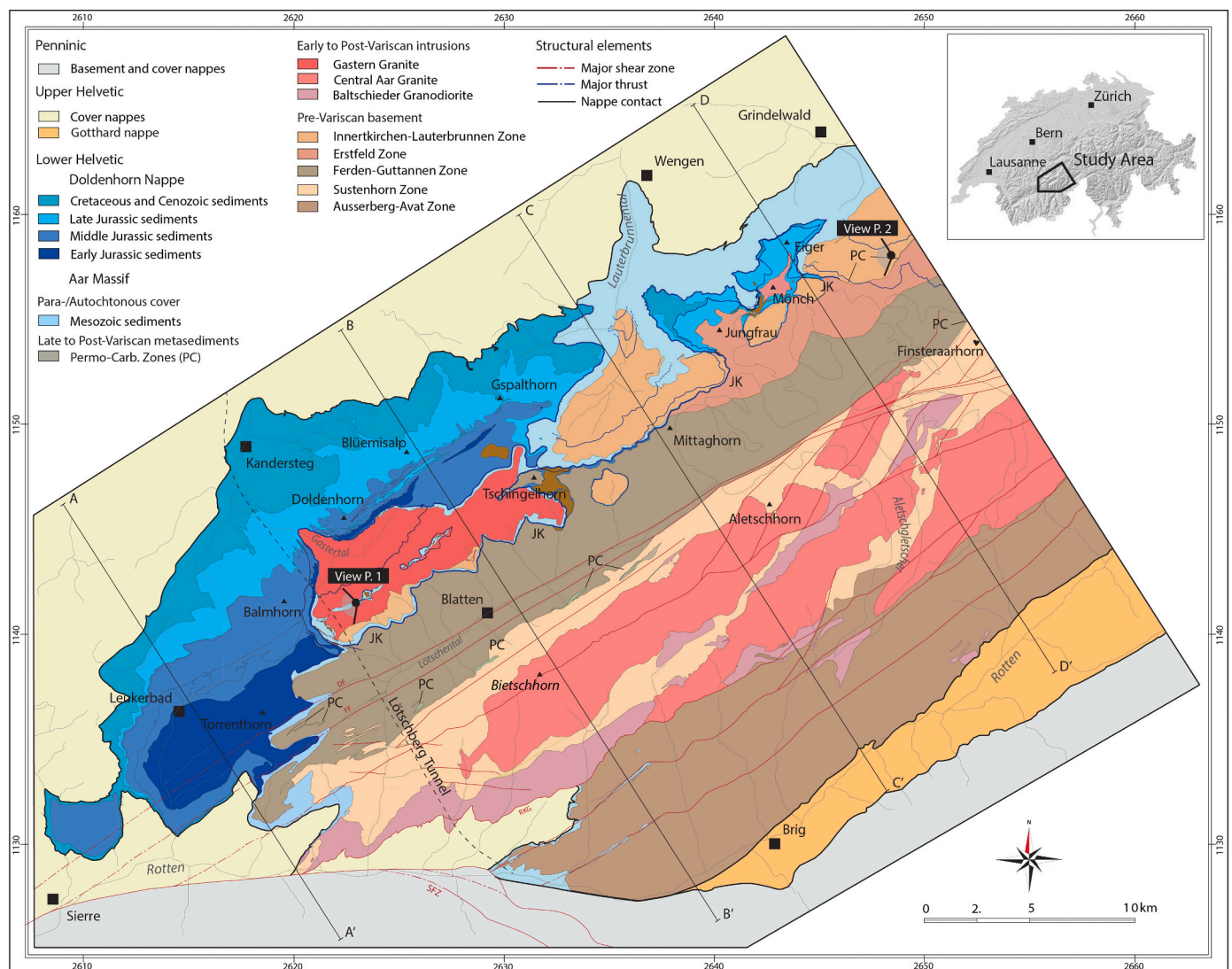


Fig. 1. Geological map of the investigated area (see Appendix A for details on data compilation). On the map are indicated: geographic locations, the profile traces of Fig. 4, the viewpoints (P.1 and P.2) of Fig. 3, trace of the Lötschberg Railway Tunnel, the locations of the thin sediment wedge called 'Jungfrau Keil', and the location of the Permo-Carboniferous troughs (PC).

Nappe as an ideal laboratory that links field-based structural and analogue-numerical modelling studies for an improved understanding of the evolution of a fold-and-thrust belt.

2. Geological setting

The Helvetic nappe stack in the Central Swiss Alps represents a classical fold-and-thrust belt. It has been intensively studied during the last century and present, because it preserves one of the best-documented ancient rifted passive margin (e.g. Heim, 1922; Ramsay, 1981; Burkhard, 1988; Pfiffner, 1993; Schmid et al., 2004; Cardello and Mancktelow, 2014). This litho-tectonic unit is mainly composed of carbonate-dominated Mesozoic and Palaeogene sediments that are partially or completely detached from their original pre-Triassic crystalline basement.

Throughout the last Alpine cycle, the nappe stack was formed during the compression and related inversion of the basement-cover systems that constituted the proximal part of the European passive continental margin (Burkhard, 1988; Epard, 1990; Steck, 2008; Pfiffner, 2015). The Doldenhorn Nappe, which is the focus of this study, is one of the lowermost units of these nappes. It crops out in a 150 km² area on the western margin of the Aar/Gastern Massifs, which are one of the External Crystalline Massifs of the Alps (Fig. 1). The Doldenhorn Nappe exhibits distinct 3D structural features such as lateral variation of the geometry and deformation style (Epard, 1990).

The crystalline basement of the Aar Massif is mainly composed of pre-Variscan polycyclic metamorphic gneisses and migmatites (Abrecht, 1994; Berger et al., 2017; Herwegh et al., 2020). These gneiss units were intruded by Variscan to post-Variscan plutons. The intrusion of the magma was associated with the formation of Permo-Carboniferous half-graben structures, which were then filled with volcanoclastic sedimentary sequences. The overlying Doldenhorn Nappe units were deposited during the Mesozoic within a basin situated on the European extended margin. The geometry of this basin and the sedimentation pattern therein were constrained by extensional Mesozoic faults (Burkhard, 1988; Pfiffner, 2015). The sedimentary units that formed in this basin consist of a succession of limestones, marls, shales, and sandstones (Fig. 2).

The deformation of the Doldenhorn Nappe started during Oligocene times (~30 Ma; Table 1) and was localized at different levels in the sedimentary units, and in the basement units (Table 1). Between 30 and 20 Ma, the basin from which the Doldenhorn Nappe originated (Doldenhorn Basin) was inverted and incorporated into the Alpine edifice, which resulted in the formation of a large-scale recumbent, isoclinal fold thrustured over the crystalline basement (Fig. 3; see also Herwegh and Pfiffner, 2005). This phase, when the sediments were partly detached from the basement, has been referred to as Kiental deformation (Table 1 and references therein). At ~22 Ma further shortening led to the onset of a multistage and pervasive deformation sequence within the crystalline basement units of the future Aar/Gastern Massifs. First, between 22 and 12 Ma, during the Handegg phase (Table 1, and references therein), the buoyancy-driven sub vertical extrusion of the Aar Massif occurred, which is expressed by steep-reverse shearing and faulting. This led to exhumation of the basement units and passive up doming of the entire nappe stack (Herwegh and Pfiffner, 2005; Cardello et al., 2016a; Herwegh et al., 2017, 2020). Secondly, after the Handegg phase, between 12 Ma and today, the northern part of the Aar/Gastern Massifs experienced a period of NW-vergent thrusting along moderately SE dipping shear planes that cut through basement-cover contacts (Pfaffenhopf phase; Table 1, and references therein). This deformation was associated with the generation of steep shear zones and faults with a dextral strike-slip sense of shear in the central and southern part of the Aar Massif (Oberaar phase of Wehrens et al., 2017; Table 1, and references therein).

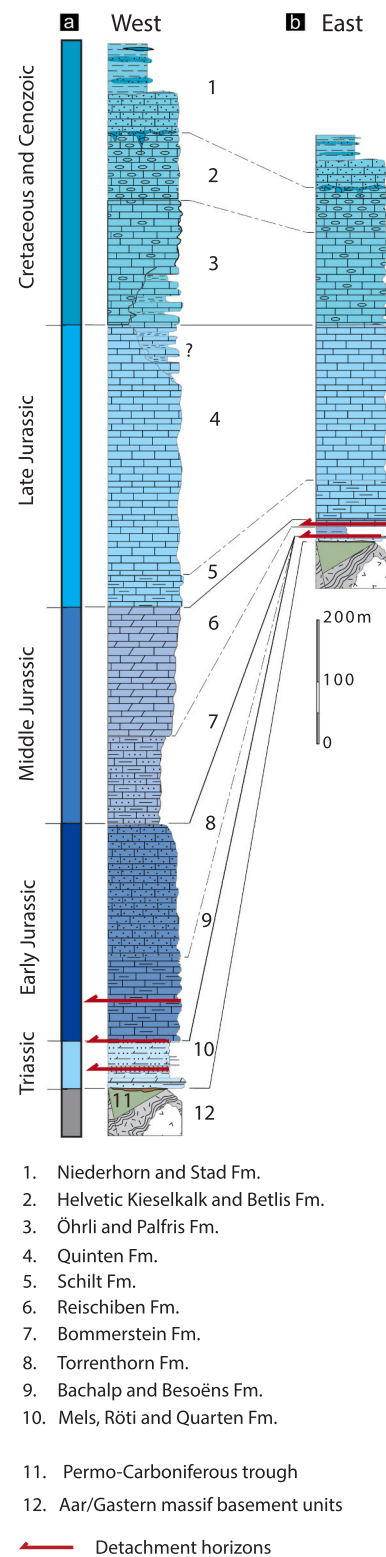


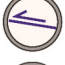



Fig. 2. Synthesized stratigraphic columns of the Doldenhorn Nappe in the West (A) and East (B) of the investigated area. The major detachment horizons are indicated with red arrows. Stratigraphic names are from the Lithostratigraphic Lexicon of Switzerland (<https://www.strati.ch/en/tectonic/aar-gastern/aar-massiv>) and data were compiled from Krebs (1925); Masson et al. (1980); Krayenbuhl and Steck (2009); Ziegler and Isler (2013); Mair et al. (2018) and references therein. (For interpretation of the references to colour in this figure legend, the reader is referred to the web version of this article.)

Table 1

Literature compilation of deformation phases that characterized the investigated area during the late-stage Alpine orogeny (30 to 0 Ma).

Age (Ma)	Deformation phase	Deformed units	Deformation style	References
~30–20	 Kiental	Sedimentary cover (<i>Doldenhorn Nappe</i>)	Top- to NW-dominated thrusting and folding	Burkhard, 1988; Huon et al., 1994; Herwegh and Pfiffner, 2005
22–12	 Handegg	Basement (<i>Aar/Gastern Massifs</i>)	Steep-reverse S-dipping shearing and faulting	Wehrens et al., 2016; Berger et al., 2017
< 12	 Pfaffenchoepf	Basement (<i>Aar/Gastern Massifs</i>)	NW-vergent thrusting along moderately SE dipping shear planes (Northern units)	Wehrens et al., 2017; Mair et al., 2018; Herwegh et al., 2020
< 12	 Oberaar	Basement (<i>Aar/Gastern Massifs</i>)	Dextral Strike-slip shearing and faulting (Southern units) – Negligible-	Wehrens et al., 2016, 2017; Herwegh et al., 2020

3. Methods

In order to reconstruct the tectonic evolution of the Doldenhorn Nappe during different stages of continent-continent collision, it was essential to construct a structurally consistent large-scale 3D geological model of the investigated area. To achieve this goal, a 2D dataset was compiled and validated within a geographic information system software (ESRI's ArcGIS, v.10.8). Then the 3D tectonic architecture was modelled with the software Move™ by Petroleum Experts (Petex, v.2019.1). In a second stage, four geological cross-sections throughout the investigated area were retro-deformed thereby performing area and line balancing in the GIS environment. Finally, the 4D reconstruction of the Doldenhorn Nappe was achieved using the Move™ software, thereby applying interpolation and meshing techniques between the retro-deformed cross-sections for four specific time intervals.

3.1. Geological data compilation, establishment of stratigraphic model and fieldwork

A detailed geological bedrock map of the investigated area was constructed by compiling and revising geological, stratigraphic and structural information from previous maps (for a review of the compiled dataset, see Appendix A). The mapping was conducted at the 1:25000 scale and considered the major stratigraphic and tectonic boundaries of the cover and basement units, it included removing the Quaternary cover and interpreting the trend of the underlying contacts. For simplicity, the stratigraphic suite of the Doldenhorn Nappe was synthesized into five larger units (Fig. 2): (i) the Triassic units (Mels, Röti and Quarten Formations) composed of dolomites, shales sandstones, and evaporites; (ii) the Late Triassic to Early Jurassic units (Besoëns, Bachalp and Torrenthorn Formations) composed of marly, spary and sandy limestones; (iii) the Middle Jurassic units (Bommerstein and Reischiben Formations or relatedly the Dugny and Erzegg Formations) made up of calcareous breccia and sandstones; (iv) the Late Jurassic units (Schilt and Quinten Formations) that comprise limestones and thin marly layers; and (v) the Cretaceous and Palaeogene units (Palfris, Öhrli, Betlis and Helvetic Kieselkalk Formations and siderolithic deposits unconformably overlaid by Stad and Niederhorn Formations) that are composed of biogene and spary limestones, and layers of sandstones and shales. The autochthonous sedimentary cover of the Aar/Gastern Massifs was not subdivided (see legend Figs. 1 and 2). Here we focus on changes in sediment thickness, for additional information, e.g. on sedimentary facies, we refer to the original studies (Krebs, 1925; Rohr, 1926; Masson et al., 1980 and references therein). These simplifications allow distinguishing the main stratigraphic horizons, which builds the basis to obtain a more comprehensive overview of the lateral structural and sediment thickness variations that occur within the nappe.

The entire dataset was combined and validated in an effort to generate a consistent geological map of the study area (Fig. 1). This was accomplished using high-resolution orthophotos (SwissImage with a

raster resolution of 0.25×0.25 m; provided by swisstopo), a high-resolution digital elevation model (DEM; swiss ALTI3D with a down-sampled raster resolution of 2×2 m, version 2013 provided by swisstopo), and hillshade maps, which served to verify and update geological boundaries and structures. A lineament map was generated on remotely sensed images with the aim to expand the structural dataset following the workflow of Baumberger et al. (2022). All data were verified in the field at key locations through mapping and collection of structural field data (see Appendix A).

3.2. 3D geological modelling

Due to the lack of borehole and underground information, 3D geological modelling in mountainous environment is a challenging task. However, high relief, scarce vegetation, and underground data offered by the Lötschberg railway tunnel (see trace in Fig. 1, Ziegler and Isler, 2013) and seismic studies (Pfiffner et al., 1997) render the investigated area prone to advanced surface-based 3D modelling. All available 2D data (mapped boundaries and structures, strike and dip data, Lötschberg tunnel and seismic sections) were loaded with the software Move™ and projected on a DEM (raster resolution 35×35 m). Then, throughout the area, a dense regularly spaced (500 m) network of NNW-SSE striking constructional cross-sections was generated, where, with 3D projection techniques and dip information, the tectonic and geological boundaries were digitized with lines (in an along-length sampling interval of 25 m; for more detailed information on the modelling procedure, see Appendix A). By applying 3D interpolation and meshing techniques (i.e. the spline curve method), lithological and structural boundaries were interpolated between the DEM surface and cross-sections to generate 3D surfaces for each horizon of the model. Following this approach, the 3D model of the investigated area considers field observations, structural analysis at the outcrop scale, tunnel and literature data, and large-scale seismic profiles.

3.3. Cross-section restoration and 4D reconstruction

To reconstruct the tectonic evolution of the Doldenhorn Nappe during the Alpine collision (30–0 Ma), four NNW-SSE cross-sections (see traces α , β , γ , δ in Fig. 4; note that traces are overlying with A-A' to D-D' cross sections, but they are more extended) were retro-deformed by performing line- (i.e. for the basement-cover contact) and area-balancing (i.e. for the Doldenhorn Nappe units) in GIS (see Appendix B). Additionally the top basement was restored assuming a precollisional geometry of the Doldenhorn Basin located on an asymmetric half-graben on the proximal part of the European passive continental margin, being bent by $\sim 10^\circ$ (Nibourel et al., 2018, 2021a) underneath the tectonically active boundary of the overriding plate. The resulting geometry and final depth is constrained by this angle and retrodeformation of the previously mentioned structures. (see Appendix B for detailed information on the restoration). The retro-deformation procedure was

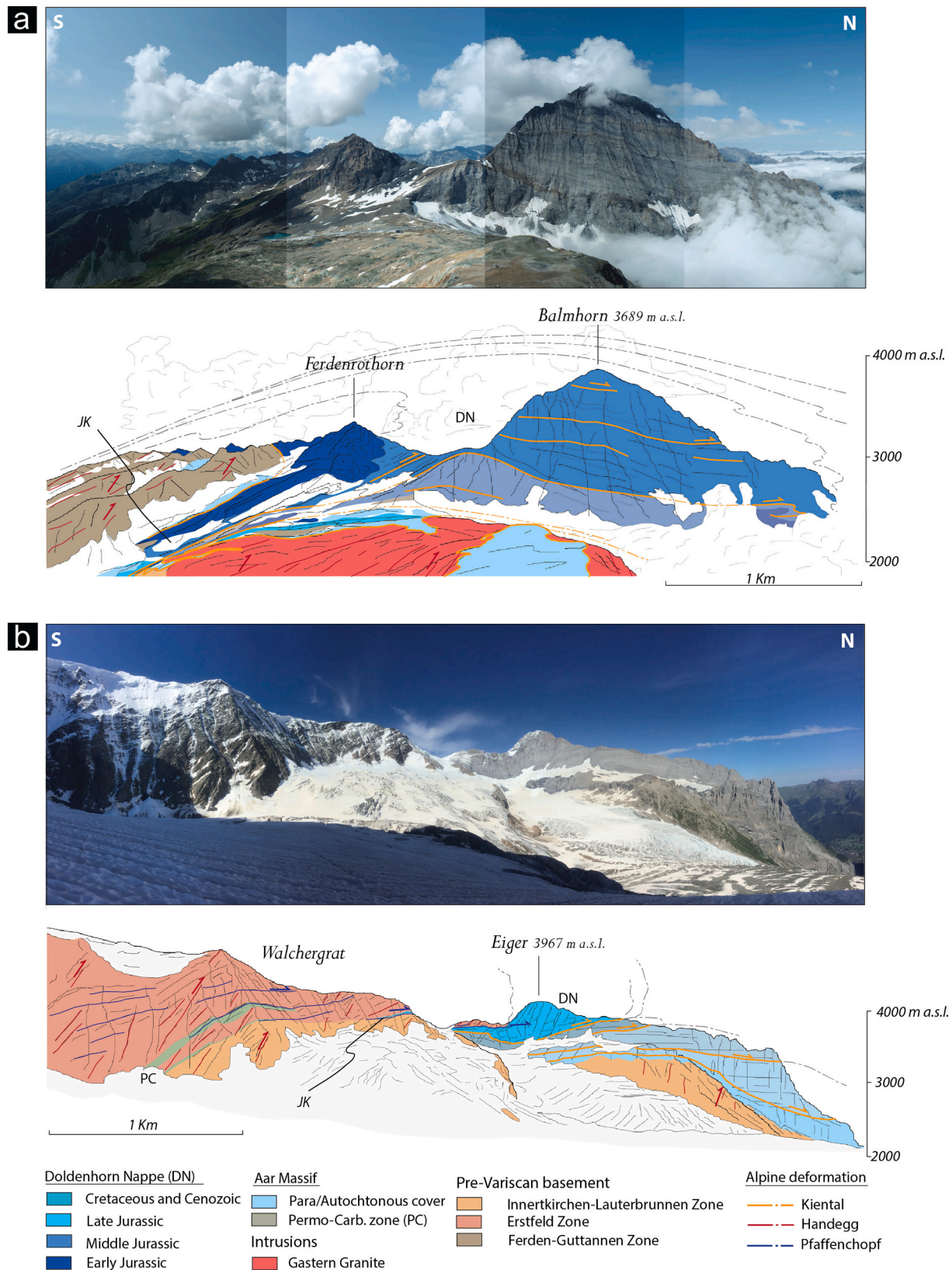


Fig. 3. Panoramic view and relative geological interpretation of two key locations of the Doldenhorn Nappe (DN) and basement units. (A) View of the east side of the Balmhorn and Ferdenrothorn (Viewpoint 1, Fig. 1). The basement units reach 3000 m a.s.l. and the DN consist of a large-scale recumbent fold that lies over the exhumed basement units. A thick wedge of the DN sediments, named Jungfrau Keil (JK), is present between the basement units. (B) View of the east face of the Eiger and the Walchergrat (Viewpoint 2, Fig. 1). The basement units exceed the 4000 m a.s.l. and driven by Pfaffenchopf structures are thrust towards the north. The JK is pinched between the basement units and continues into a thrust Permo-Carboniferous zone (PC). The DN is a small-scale fold that lies over an imbricate of autochthonous sediments of the Aar Massif.

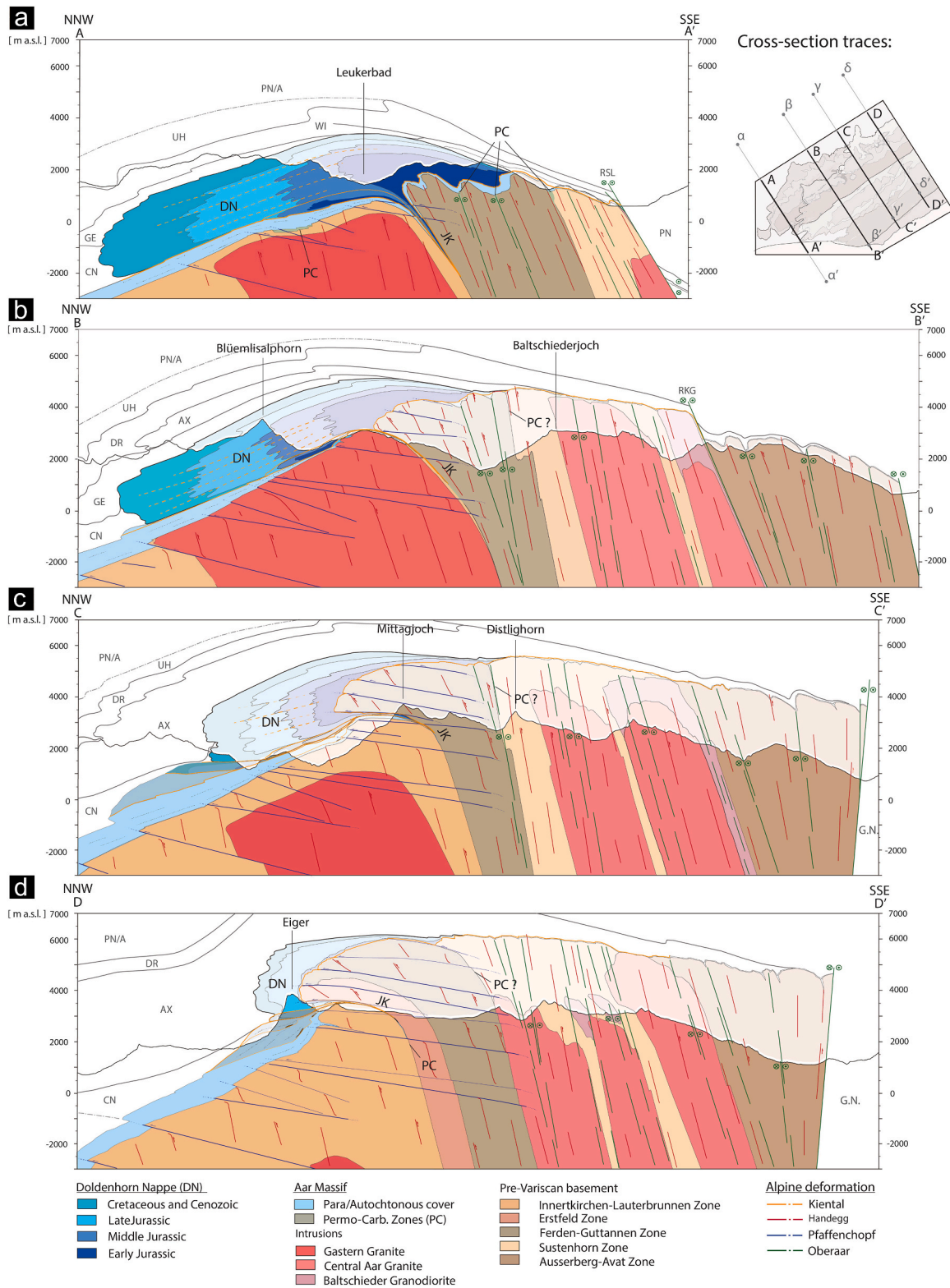


Fig. 4. Cross-sections through the investigated area (see Fig. 1 for cross-sections traces). In the profiles are indicated: the structural deformation phases, the overlying Helvetic nappes (GE, Gellihorn; WI: Wildhorn; AX: Axen; DR: Drusberg; UH: Ultrahelvetic), including the Cenozoic sediments (PN/A) and the Penninic and Austro-alpine sediments (CN) and. In section A-A' and B-B' the outline of the overlying upper Helvetic nappes were modified after Herwegh and Pfiffner (2005) and Hänni and Pfiffner (2001) respectively. (A) Section A-A' where DN is a large-scale recumbent fold with a thick normal limb and a thin and intensively deformed inverted limb. (B) Section B-B', gradual exhumation and thrusting of the basement units, the DN maintains still the shape of a recumbent fold. (C) Section C-C': more pronounced exhumation and thrusting of the basement units. In the North, lies a stack of imbricates of Autochthonous sedimentary cover. (D) Section D-D' the exhumation and thrusting towards the North of the basement units are more prominent compared to what is observable in section AA'. The DN consists of a small-scale fold and the basement units are thrust in the core of the nappe.

performed according to the following four time steps: *Today to 12 Ma*: retro-deformation of the displacement along the youngest northwest vergent thrust deformation of the Aar Massif (Pfaffenchoepf structures; Table 1); during this time, a strike-slip movement was also active in the basement units of the Aar Massif (Oberaar phase, Table 1; Wehrens et al., 2016, 2017). In this study however, its contribution to the overall shortening and nappe evolution was considered negligible since the related deformation affected the basement and sedimentary units of the southern most parts of the massif where no Doldenhorn Nappe units accumulated, implying therefore maintenance of the Doldenhorn Nappe volumes throughout the entire Alpine deformation. *12 to 20 Ma*: retro-deformation of the reverse-steep fault related exhumation of the Aar Massif (Handegg phase; Table 1) and of the overlying nappe stack, while using the basement-cover contact as marker horizon. Despite the large degree of exhumation caused by the Handegg phase, the topographic mean elevation along the sections was kept constant, as stated by Campani et al. (2012) and Schlunegger and Kissling (2015). *20 to 30 Ma*: retro-deformation of the Kiental phase (Table 1). Herein, the location of Permo-Carboniferous zones and sediment wedges (Figs. 1, 3 and 4) served as a marker for potential locations of *syn*-rift faults controlling the opening of the Doldenhorn Basin (more information provided in Appendix A). Subsequently, the cross-sections representing these stages were digitalized in Move™. A 3D model of each retro-deformation stage was then generated by applying 3D interpolation and meshing techniques (spline curve method) within the digitalized sections.

4. Results and interpretation

In this section, a structurally consistent characterization of today's architecture of the Doldenhorn Nappe and Aar/Gastern Massifs is presented emphasizing the along strike variations in the sedimentary and basement units from West to East of the investigated area. Subsequently,

the results of the western- and eastern-most cross-sections restoration (respectively α - α' , and δ - δ' ; see traces in Fig. 4) are discussed in stages punctuated by the major three Alpine deformation phases (Kiental, Handegg, and Pfaffenchoepf; Table 1), and highlight the along-strike discrepancies throughout this evolution. Finally, by combining the obtained results, an estimation of the total horizontal shortening and maximum vertical uplift along the restored cross-sections through the investigated area is derived.

4.1. Field data and 3D geological model of Doldenhorn Nappe and Aar/Gastern Massifs

The sedimentary units of the Doldenhorn Nappe show a distinct spatial distribution above the western edge of the Aar Massif basement units. Primarily, the overall thickness of the Doldenhorn Nappe units drastically decreases from the West to the East parallel to the strike of the nappe (see Figs. 1 and 2). The Early Jurassic units, which are 350 m thick in the West (Fig. 2; Masson et al., 1980; Krebs, 1925; Krayenbuhl and Steck, 2009) of the investigated area, progressively thin out and disappear in the East. The thicknesses of the Middle Jurassic units also decrease from 350 m in the West (Masson et al., 1980; Krebs, 1925) to 30 m in the East (Mair et al., 2018). Similarly, the Late Jurassic and Cretaceous/Paleogene units also taper off from 450 m and 460 m to 310 m and 300 m, respectively (Masson et al., 1980; Mair et al., 2018).

From a structural point of view, in the West the Doldenhorn Nappe is a large-scale (distance front to core of 11 km) recumbent isoclinal fold (Fig. 3a, see also Herwegh and Pfiffner, 2005) with a 2.0 km-thick normal limb and a 0.7 km-thick inverted limb (Fig. 4a). The Kiental thrust planes, along which the emplacement of the nappe occurred, are bent parallel to the basement-sedimentary cover contact with an average orientation (dip direction/dip angle) of 176/20 (Fig. 5a). Below the Doldenhorn Nappe and just above the basement lie the 50 to 500 m-

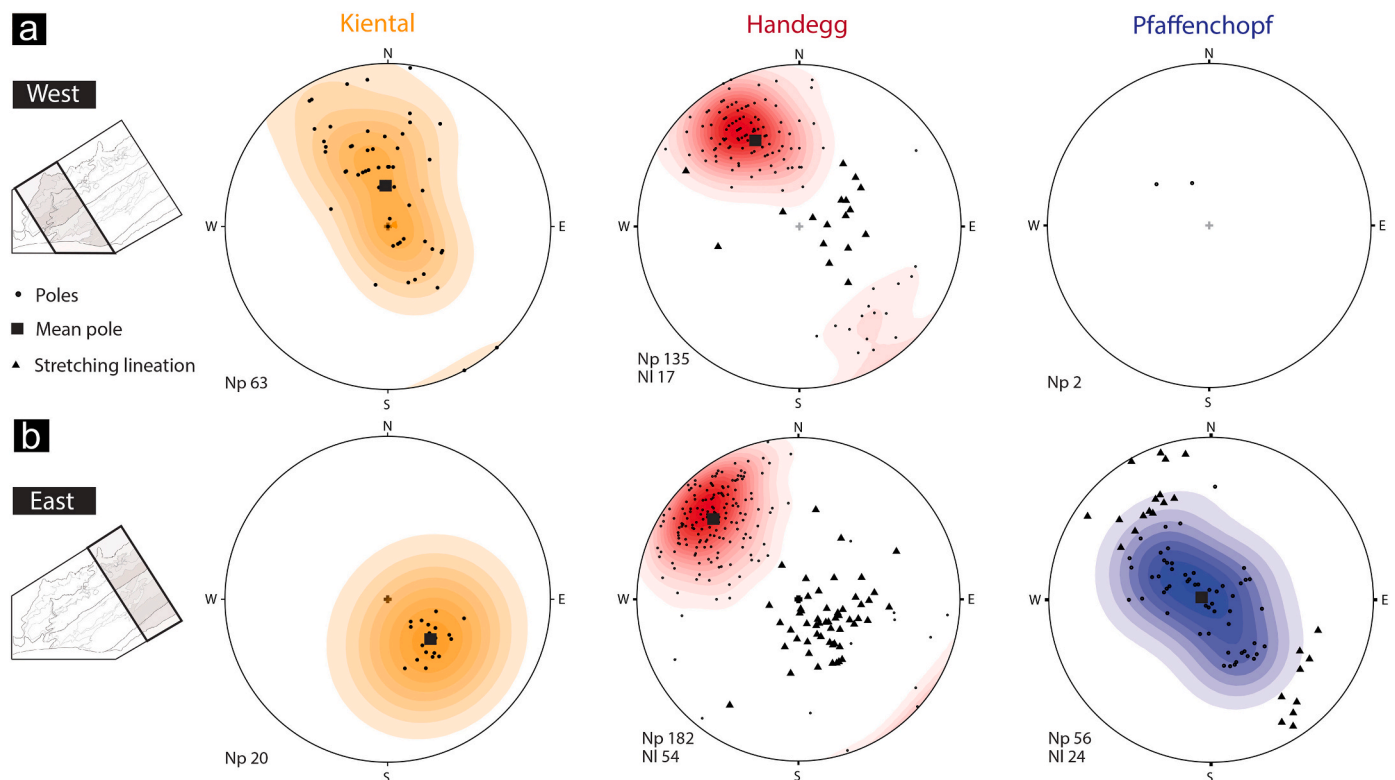


Fig. 5. Structural field data (poles and mean poles of the fault and thrusts planes) of the deformation structures in the sediments of the DN (Kiental) and basement units of the Aar Massif (Handegg and Pfaffenchoepf). To highlight the differences between the East and West of the investigated area the sets of measurements are subdivided in two-dataset. (A) dataset of the measurements of the western regions of the investigated area, representative for the profile A-A'. (B) Dataset of the measurements in the East of the investigated area, representative for the profile D-D'.

thick autochthonous sediments of the Aar Massif.

In contrast, in the East, the Doldenhorn Nappe displays reduced dimensions with smaller-sized fold structures, much shorter limbs (distance front-core ~ 2 km) as well as a 1.5 km-thick normal limb and a 0.5 km-thick inverted limb. Here, the Kiental thrust planes gently dip towards the NW with a mean orientation of 314/30 (Fig. 5b). Below the Doldenhorn Nappe lies an imbricate stack mainly consisting of the para-autochthonous sedimentary cover of the Aar massif (Figs. 3b and 4d; see also Mair et al., 2018). These imbricates are bound by Kiental thrusts locally incorporating decametre-sized slivers of the Aar Massif basement rocks (see Mair et al., 2018).

The basement units of the western edge of the Aar Massif progressively gain relief moving from the western to the eastern part of the investigated area. In the West, the basement rocks reach an elevation of ~ 3000 m a.s.l. (Fig. 3a). The Handegg structures, along which exhumation of these units was achieved, dissect the basement rocks with SE-dipping semi-brittle to brittle faults that evolved from former ductile shear zones (see Wehrens et al., 2016; Berger et al., 2017; Mair et al., 2018; Herwegh et al., 2020). The average orientation (dip direction/dip angle) of the fault planes is 153/50. Shear sense indicators on down-dip stretching lineations of these faults indicate preferential upward movements of the southern blocks (Fig. 5a). In the eastern part of the investigated area, the basement units exceed an elevation of 4200 m a.s.l. The mean orientation (dip direction/dip angle) of the Handegg structures is 133/62, with down-dip stretching lineations with kinematic indicators of an up movement of the S-block (Fig. 5b).

Furthermore, over the entire northern section of the crystalline units, the Handegg structures are cut and offset by younger Pfaffenchof thrust planes that have an NW-vergent and moderately SE-dipping orientation (see Wehrens et al., 2017; Mair et al., 2018; Herwegh et al., 2020). Note that such structures in the NW portion of the investigated area are not well developed at the surface (Fig. 5a), but they occur at depth as they were identified in the Lötschberg railway tunnel and on seismic profiles

(Ziegler and Isler, 2013; see Pfiffner et al., 1997, NEAT 9001 and Line W1; Fig. 4a). However, in the NE part of the investigated area, these structures occur both at the surface (Mair et al., 2018) and at depth (Pfiffner et al., 1997, Line C1; Herwegh et al., 2020; Figs. 3b and 4d). Along the Pfaffenchof thrust planes (mean values: 105/05; Fig. 5b) the southern basement units (Erstfeld and Ferden-Guttannen Zones; Fig. 1) are thrust over the northern basement units (Gastern Granite and the Innerkirchen-Lauterbrunnen Zone; Figs. 1, 3b, 4c, d, and 6).

Pinched between the mentioned basement units lies a thin wedge of Doldenhorn Nappe sediments, known in literature as ‘Jungfrau Keil’ (e.g. Krayenbuhl and Steck, 2009), which is traceable along the entire strike of the nappe (Fig. 1). In the West, the ‘Jungfrau Keil’ is associated with Permo-Carboniferous units (Fig. 3a) and extends further than 750 m a.s.l. depth, indicating a today’s minimum wedge length of 1650 m. In contrast, in the East, the ‘Jungfrau Keil’ displays much smaller dimensions with a vertical extent of a few hundreds of meters only. Here the ‘Jungfrau Keil’ culminates in a Permo-Carboniferous zone (Fig. 3b).

4.2. Cross-section restoration and tectonic evolution

To unravel in space and time how the Doldenhorn Nappe reached its current structural organization during Alpine deformation, four NNW-SSE geological cross-sections (α - α' , β - β' , γ - γ' , δ - δ' ; see also traces in Fig. 4) were retro-deformed. In the following paragraphs we present the results of the retro-deformation of sections α - α' and δ - δ' as evolutionary steps, starting from the initiation of Alpine deformation to the present-day configuration (Figs. 7 and 8; the retro-deformed sections β - β' and γ - γ' are available in Appendix B). Finally, the resulting total horizontal shortening and maximum vertical uplift of each transect (α , β , γ , δ), recorded by the Doldenhorn Nappe and basement-cover interface during the different evolutionary steps is then summarized in the plots of Fig. 9.

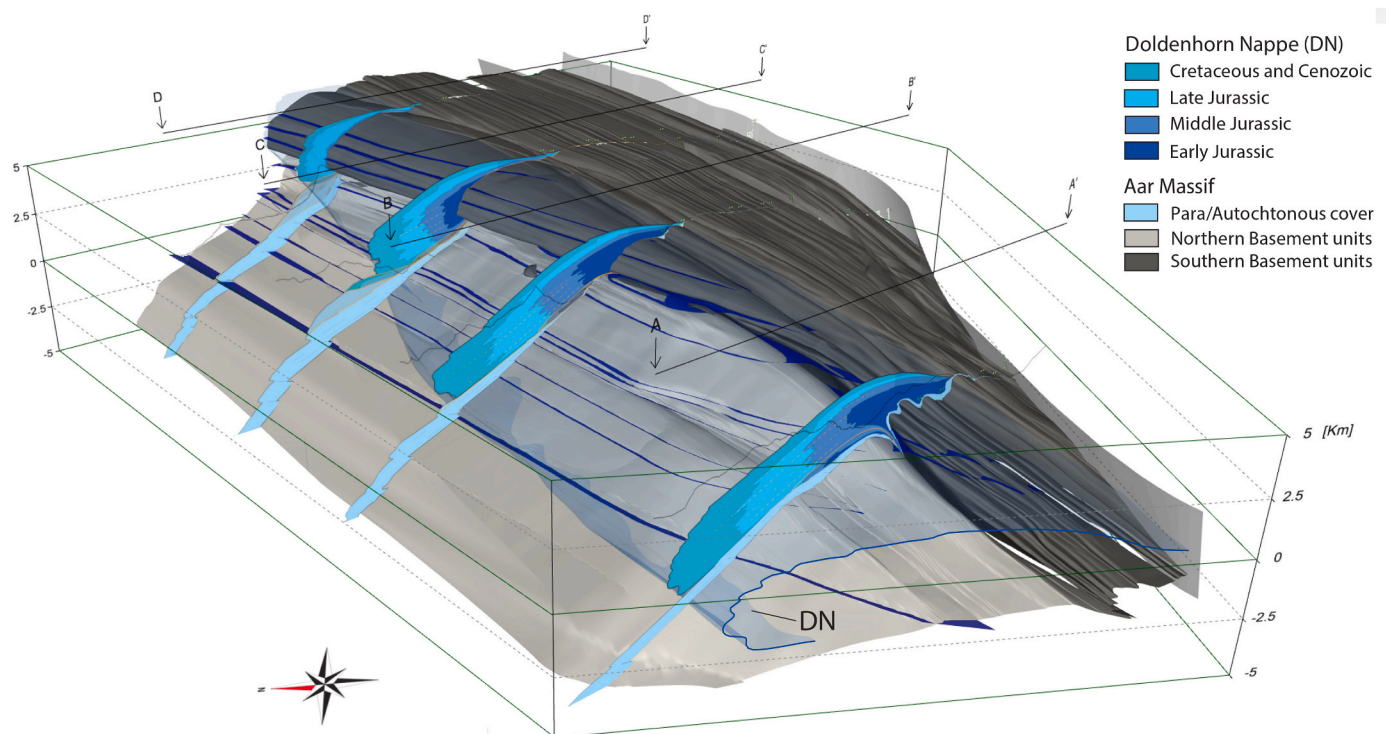


Fig. 6. View from the West of the 3D model of the current structural disposition of the DN and basement units. In this image, highlighted by the four cross-sections A, B, C, D (Fig. 4), the along-strike changes that occur within DN are illustrated. The basement units are merged into two major groups: the southern basement units (dark gray) and the northern basement units (light gray). The units are gradually exhumed from the West to the East at higher elevations and thrust towards the North.

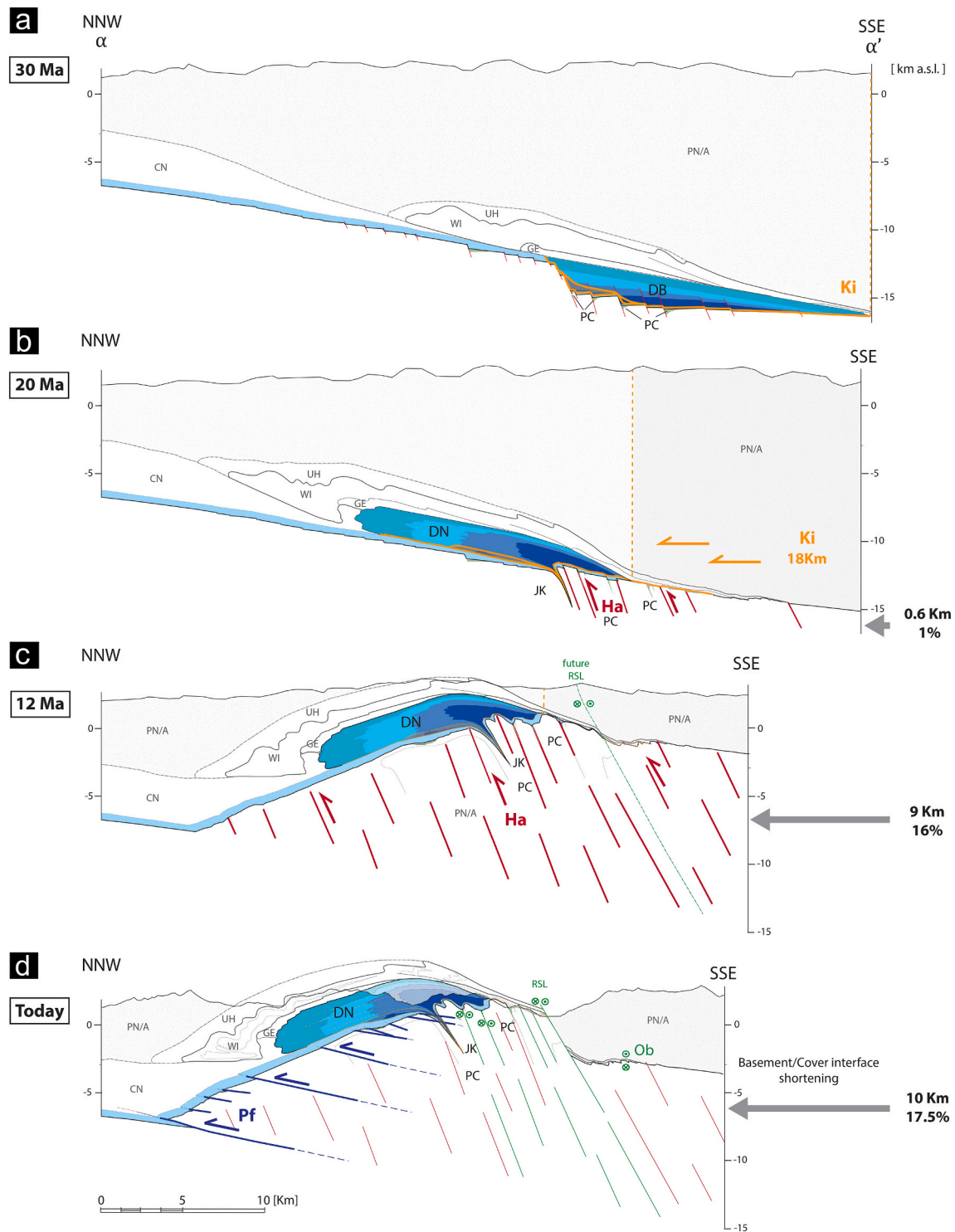


Fig. 7. Cross-section restoration of the α - α' transect from 30 Ma to today. At each deformation stage, thicker lines and stronger colors highlight the corresponding deformation phase. (A) The Doldenhorn Basin (DB) at 30 Ma is located in a half-graben of the European passive continental margin. The DB is buried below the already emplaced Helvetic nappe stack (UH: Ultrahelvetic units; WI: Wildhorn nappe; GE: Gellihorn nappe) and Cenozoic sediments (CN) in the north. Above lies a thick wedge of Penninic and Austroalpine units (PN/A). (B) DN at 20 Ma. Handegg deformation (Ha) in the southern basement units is indicated in red colors. (C) Exhumation of the basement units and consequent up-doming of the nappe stack induced by the Handegg deformation at 12 Ma. (D) Current structural disposition of the DN and basement units. Thrusting of the basement units towards the north documented by the Pfaffenchof structures (Pf). (For interpretation of the references to colour in this figure legend, the reader is referred to the web version of this article.)

4.2.1. Restoration α - α'

The deformation and emplacement of the Doldenhorn Nappe along the α - α' section was divided into four main stages as follows.

Time step 30 Ma (Fig. 7a). The Doldenhorn Basin sat in a half-graben

structure on the former passive continental margin of the European plate and was bent by $\sim 10^\circ$ (Ebert et al., 2008; and Nibourel et al., 2018, 2021a) underneath the tectonically active boundary of the overriding units (see Appendix B for additional information). The basin was 24 km

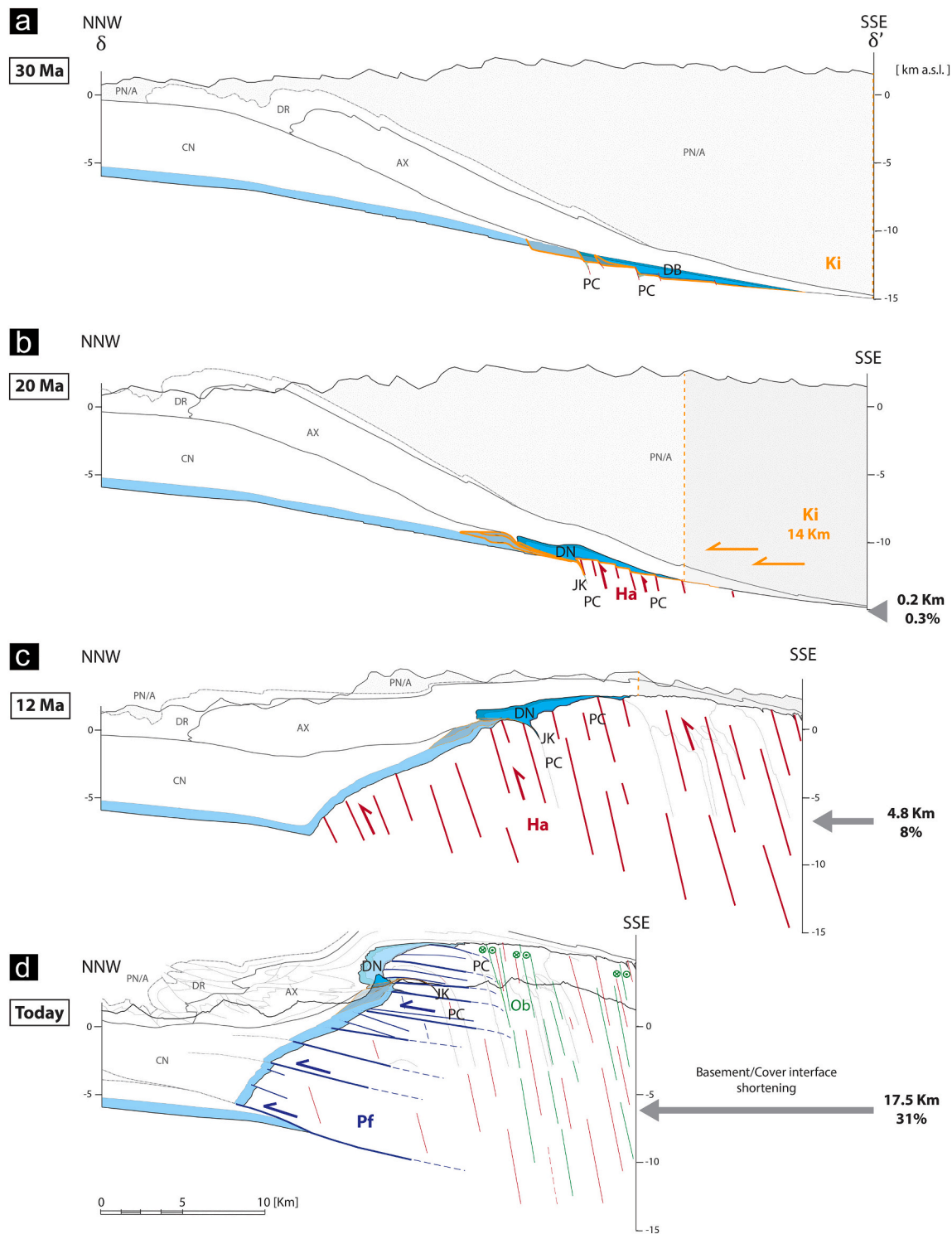


Fig. 8. Cross-section restoration of the δ - δ' transect from 30 Ma to today. At each deformation stage, the corresponding active deformation phase is highlighted by larger line weight and stronger colour. (A) The Doldenhorn Basin (DB) at 30 Ma is located in a half-graben of the European passive continental margin. The DB is buried below the already emplaced Helvetic nappe stack (AX: Axen nappe; DR: Drusberg nappe) and Cenozoic sediments (CN) in the north. Above lies the wedge of Penninic and Austroalpine units (PN/A). (B) At 20 Ma, due to the Kiental deformation the DN is extruded into a small amplitude fold, and in the north lies a stack of three slices of autochthonous sediments. Handegg deformation (Ha) in the southern basement units is indicated in red colors. (C) Exhumation of the basement units and up-doming of the nappe stack induced by the Handegg deformation at 12 Ma. (D) Current structural disposition of the DN and basement units. Significant thrusting of the basement units towards the north driven by the Pfaffenchoepf structures (Pf). (For interpretation of the references to colour in this figure legend, the reader is referred to the web version of this article.)

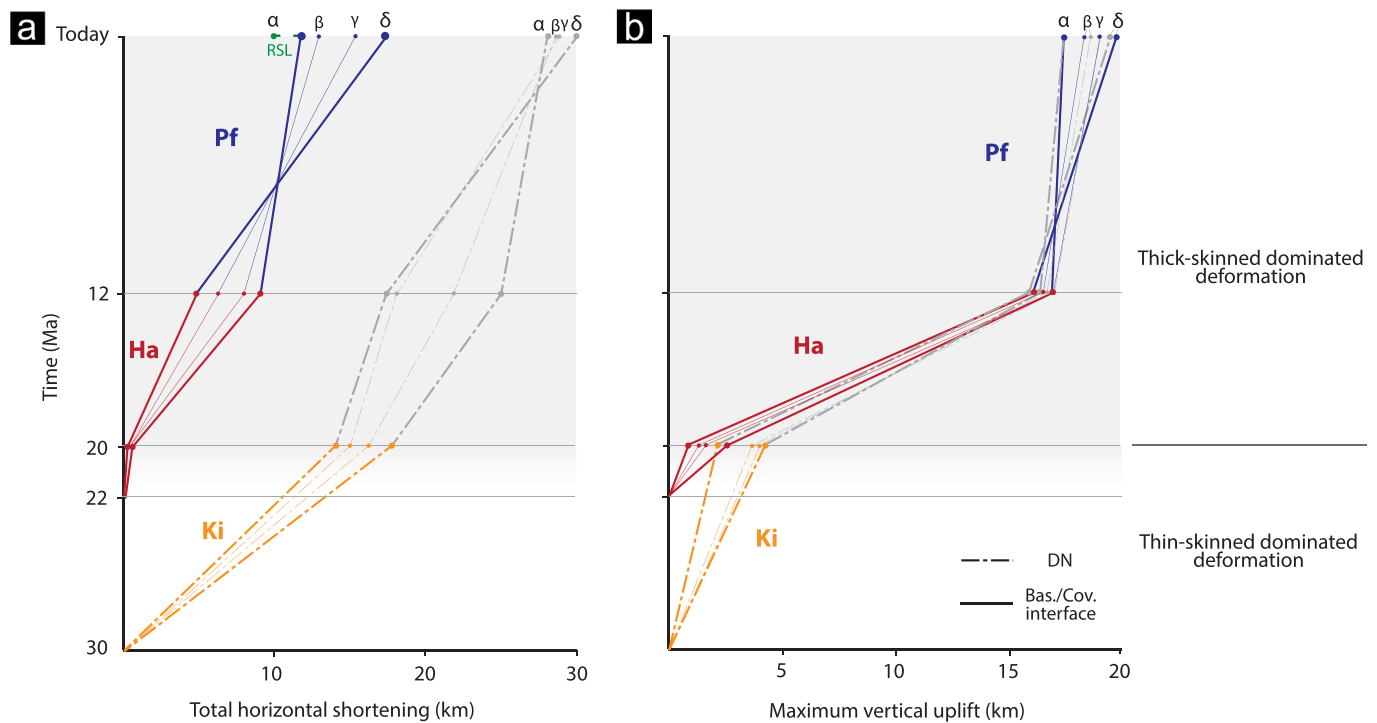


Fig. 9. Plots of the total horizontal shortening (A) and maximum vertical uplift (B) recorded by the Doldenhorn Nappe (DN) and basement-cover interface (dashed line and simple line respectively) in the sections α , β , γ , δ during the restoration time intervals. (A) Horizontal shortening recorded by DN sediments induced by the Kiental phase (orange line 30 to 20 Ma) and by the shortening localized in the basement units (gray line 20 Ma to today). Horizontal shortening in the basement units was initiated at 22 Ma. This thick-skinned deformation stage results in a ~12 to 17.5 km horizontal shortening of the basement-cover interface, and 28 to 30 km of the DN. (B) Maximum vertical uplift recorded by the DN and basement-cover interface. The maximum total vertical uplift recorded in each section ranges from 18 to 20 km both for the DN and for the basement-cover interface.

long and dissected by several normal faults often related to smaller-scale Permo-Carboniferous half grabens (see Appendix A). In the North, the major escarpment displayed a throw of 2 km, and the sedimentary sequence had a maximum thickness of 2.5 km. The Doldenhorn Basin was buried at -15 km depth (see also Berger et al., 2020) below both the overlying and already emplaced Helvetic nappe stack, and a thick wedge of Penninic and Austroalpine units (Fig. 7a). A similar scenario was proposed for the Morcles and Wildhorn nappes at ~ 27 Ma (e.g. Burkhard, 1988; Cardello et al., 2019). In the mechanically weak Triassic evaporite-rich and Early Jurassic shale layers (Pfiffner, 1993; Pfiffner et al., 2011; Fig. 2; see for further details discussion Section 5.2) deformation begun to be localized, and the Kiental phase detachment horizon was developed (orange line in Fig. 7a).

Time interval 30 to 20 Ma (Fig. 7b). This interval was primarily affected by thin-skinned deformation and later by the onset of thick-skinned deformation (22 to 20 Ma). Between 30 and 20 Ma, the basin was inverted along the Kiental basal thrust (orange line in Fig. 7a, b) and the units were thrust 18 km to the NNW (Fig. 9; Burkhard, 1988; Herwegh and Pfiffner, 2005). The thrusting of the units over the crystalline basement was associated with a large-scale isoclinal fold with a thin inverted limb. With progressive shortening, the overlying nappe stack was passively folded by meso-scale to large-scale folds (Herwegh and Pfiffner, 2005; Girault et al., 2020). In the southern units of the Aar Massif, the exhumation of the basement units started at 22 Ma, triggered by basement internal steep Handegg faults and shear zones (red lines in Fig. 7b; Table 1). As already observed in the western External Crystalline Massifs (Bellahsen et al., 2014) as well as in the Central to Eastern Aar Massif (Nibourel et al., 2021a), only a few Jurassic normal faults were directly reactivated. Instead, nearby new reverse faults evolved along which the uplift of the basement in the southern-blocks was accomplished. As a consequence of this reverse faulting, thin synformal wedges of Triassic, Early and Middle Jurassic and Permo-Carboniferous

sediments formed, the strata of which were steeply dipping and locally even overturned. At the Doldenhorn Basin's border fault, the 'Jungfrau Keil', one of today's most prominent of such wedges (2.5 km vertical extent, Fig. 7b), started to develop.

Time interval 20 to 12 Ma (Fig. 7c). Thick-skinned tectonics along steeply south-dipping reverse faults and shear zones (red lines Fig. 7c) dominated the Handegg deformation stage (Table 1). Due to sequential deformation, the basement units were gradually exhumed differentially from South to North. This led to an overall 9 km horizontal shortening and an up-to ~ 17 km vertical uplift of the basement-cover interface (Fig. 9). This basement internal differential shearing and reverse faulting therefore caused an overall passive up doming of the entire overlying Helvetic nappe stack including the Doldenhorn Nappe, which resulted in the onset of formation of the dome-shaped geometry of the Aar Massif. This type of deformation was also inferred from paleo-magnetic data in the Helvetic nappes located further north of the investigated area (Cardello et al., 2016b).

Time interval 12 Ma to present-day (Fig. 7d). In contrast to the previous time interval, since 12 Ma thick-skinned horizontal tectonics defines the deformation style in the region. Flat-to-moderately SE dipping Pfaffenchof thrust planes (blue lines Fig. 7d) dissect the basement units promoting a NW-directed thrusting/shortening. The deformation is mostly localized at depth and leads to an en-bloc exhumation (Nibourel et al., 2018, 2021b) of the basement units with a 2.7 km horizontal shortening and a 1 km vertical uplift of the basement-cover interface (Fig. 9). This deformation was partially compensated (-1.7 km of shortening) by the strike slip regime with a transtensional component occurring along the Rhone-Simplon Line (RSL in Figs. 7d and 9; Grosjean et al., 2004; Campani et al., 2014). This completed the deformation sequence and led to an overall horizontal shortening of 10 km and up to ~ 18 km of vertical uplift of the basement-cover interface (Fig. 9).

4.2.2. Restoration δ - δ'

The result of the restoration of the δ - δ' section is presented in the identical time intervals of the previous sections, highlighting the differences with what was described above.

Time step 30 Ma (Fig. 8a). The Doldenhorn Basin was 16.5 km long and dissected by normal faults often related to Permo-Carboniferous half grabens. In the North, the transition to the Alemannic topographic high (Trümpy, 1952) was gradual and without a major escarpment, while the basin deposits reached a maximum thickness of 0.9 km. The Doldenhorn Basin was buried at -14 km depth below the overlying Helvetic nappe stack, and Penninic and Austroalpine wedge (Fig. 8a). In the South, the Kiental basal thrust was developed in Triassic evaporite-rich and Early Jurassic shale layers. However, towards the northern end of the basin, the thrust splayed into an in-sequence set of thrusts that also extended to the autochthonous sedimentary cover in proximity of the basin (orange lines Fig. 8a).

Time interval 30 to 20 Ma (Fig. 8b). Between 30 and 20 Ma along the sequence of Kiental thrusts (orange lines in Fig. 8a and b) with 14 km of horizontal shortening (Fig. 9), the basin was inverted and the sediments were thrust to the NNW. The resulting Doldenhorn Nappe is a small-amplitude fold with a thin inverted limb. In the north, the in-sequence set of Kiental thrusts stacked a repetition of slices of autochthonous sedimentary cover of the Aar Massif. At 22 Ma, the Handegg brittle-ductile reverse faults and shear zones were localized in the southern basement units of the basin. Permo-Carboniferous, Triassic, Early and Middle Jurassic sediments were locally pinched between the basement units as synformal sedimentary wedges. As for the previous section, at the northern end of the basin, between the border fault and the basin's basement units, the 'Jungfrau Keil' sediment wedge was generated (0.9 km vertical extent; Fig. 8b).

Time interval 20 to 12 Ma (Fig. 8c). The steep reverse faults and shear zones of the Handegg phase induced 4.8 km of horizontal shortening and an up to ~16 km of vertical uplift of the basement-cover interface (Fig. 9).

Time interval 12 Ma to present-day (Fig. 8d). Thrusting along the Pfaffenchof thrust planes started both at depth and at higher elevation along the entire northern rim of the basement units. Such deformation led to: (i) considerable steepening of the northern basement-cover interface; (ii) an en-bloc exhumation of the basement units; and to (iii), thrusting of rigid slabs of southern basement units over the northern ones, which were wedged into the core of the Doldenhorn Nappe. The Pfaffenchof thrusts accommodated 12.7 km of horizontal shortening and an additional up to 3.6 km of vertical exhumation of the basement-cover interface (Fig. 9). Thus, the deformation sequence culminated with an overall 17.5 km of horizontal shortening and up to ~20 km of uplift of the basement-cover interface (Fig. 9).

4.3. Total horizontal shortening and maximum vertical uplift

The plots in Fig. 9 display the total horizontal shortening and maximum vertical uplift recorded by the Doldenhorn Nappe and basement-cover interface in the α , β , γ , δ transects during the above-mentioned restoration time intervals. The horizontal shortening recorded by the Doldenhorn Nappe units (Fig. 9a) is induced during the Kiental phase (Fig. 9a, orange line 30 to 20 Ma; thin-skinned dominated stage) and followed by shortening localized in the basement units (Fig. 9a, gray line 20 Ma to today). Horizontal shortening in the basement units was initiated at 22 Ma. During the Handegg phase (Fig. 9, red line, 22 to 12 Ma) a differential horizontal shortening (α , large; δ , small) is observed; while during the Pfaffenchof phase an opposite trend occurs (α , small; δ , large). This thick-skinned deformation stage results in ~12 to 17.5 km horizontal shortening of the basement-cover interface, and 28 to 30 km shortening of the Doldenhorn Nappe.

On the contrary, the maximum vertical uplift recorded by the Doldenhorn Nappe and basement-cover interface (Fig. 9b) shows almost an identical trend, recording a strong uplift component during the Handegg

phase (Fig. 9b, red line, 22 to 12 Ma). This results into a total vertical uplift of 18 to 20 km both for the Doldenhorn Nappe and for the basement-cover interface in each section.

5. Discussion

The results obtained through restoring the four cross-sections in the investigated area provide crucial insights into the tectonic evolution of the Doldenhorn Nappe and Aar/Gastern Massifs during the late-stage Alpine evolution, and the broader perspective of a 4D inversion of passive continental margins. By generating a 3D model of each retro-deformation stage, it was possible to build a 4D reconstruction of the Doldenhorn Nappe. In this section, the 4D reconstruction of the Doldenhorn Nappe is discussed with a particular focus on the deformation processes and structural inheritances (e.g. Butler et al., 2006 and references therein) that controlled the large along-strike variability in the tectonic architecture of the nappe and underlying Aar/Gastern Massifs basement units. Such a reconstruction indeed allows us to establish: (i) an asymmetric Doldenhorn Basin geometry becoming shallower and shorter to the NE, (ii) the rift-related 3D extensional fault architecture whereby the asymmetric basin developed, and (iii) the structural and rheological inheritance, which controls basin inversion as well proximal domain deformation during the late-stage collision between Adria and Europe.

5.1. The Doldenhorn Basin

From a geodynamic point of view, proximal domains of rift systems or passive continental margins are characterized by weakly developed rift-related lithospheric and crustal thinning (e.g. Mohn et al., 2011; Peron-Pinvidic et al., 2013). The creation of accommodation space is, therefore, restricted to graben and half-graben basins (e.g. Wilson et al., 2001; Tugend et al., 2015). The Doldenhorn Basin (Fig. 10) was located on the proximal part of the European passive continental margin characterized in the NE by the Alemannic topographic high (Trümpy, 1952). The basin itself evolved as an asymmetric half-graben bounded in the North by an East-West striking, South-dipping rotational normal fault with a larger throw in the West (ca. 2 km) and smaller throw in the East (ca. 0.8 km). This asymmetric tectonic rifting scenario resulted in a differential formation of accommodation space that affected the disposition and stratigraphic thicknesses of the sedimentary units (Figs. 2 and 10; e.g. Dollfuss, 1965; Masson et al., 1980; Balázs et al., 2016). Indeed, the Early and Middle Jurassic units are linked to the early stages of the opening of the half-graben and therefore display fluctuations in thicknesses along strike as well as thickening towards footwalls of the normal faults of the basin. The Late Jurassic and Cretaceous/Paleogene units recorded then the late to post-rift evolutionary stage of the basin (see also Kempf and Pfiffner, 2004; Cardello and Mancktelow, 2014).

The reconstructed 3-D architecture of the Doldenhorn Basin consists of a series of NE-SW to E-W striking and SE to S dipping rotational high-angle normal faults (Fig. 10; see also Doldenhorn Basin's top-crystalline basement map 30 Ma, in Appendix B). Furthermore, as also observed in several other locations in the Aar Massif (e.g. Heim, 1922; Rohr, 1926; Krayenbuhl and Steck, 2009; Nibourel et al., 2021b), large numbers of normal faults occur in places where Permo-Carboniferous troughs are located (see more information in Appendix A; Fig. 10). The large-scale crustal architecture of the European proximal passive continental margin was dominated by a series of tilted crustal blocks, bound by high-angle Mesozoic normal faults (Masini et al., 2013). The Doldenhorn Basin was sitting in a half-graben on one of this tilted blocks, filled with wedge-shaped syn-rift sedimentary units (e.g. Pfiffner, 2015; Jaquet et al., 2018). Present-day examples of comparable geodynamic settings can be found within the mid-Norwegian, Iberian or Angola-Gabon proximal domains along the Atlantic rift system (e.g. Peron-Pinvidic et al., 2013). Geophysical studies in such proximal domains reveal that the bulk crust is only slightly thinned and the subsidence-related

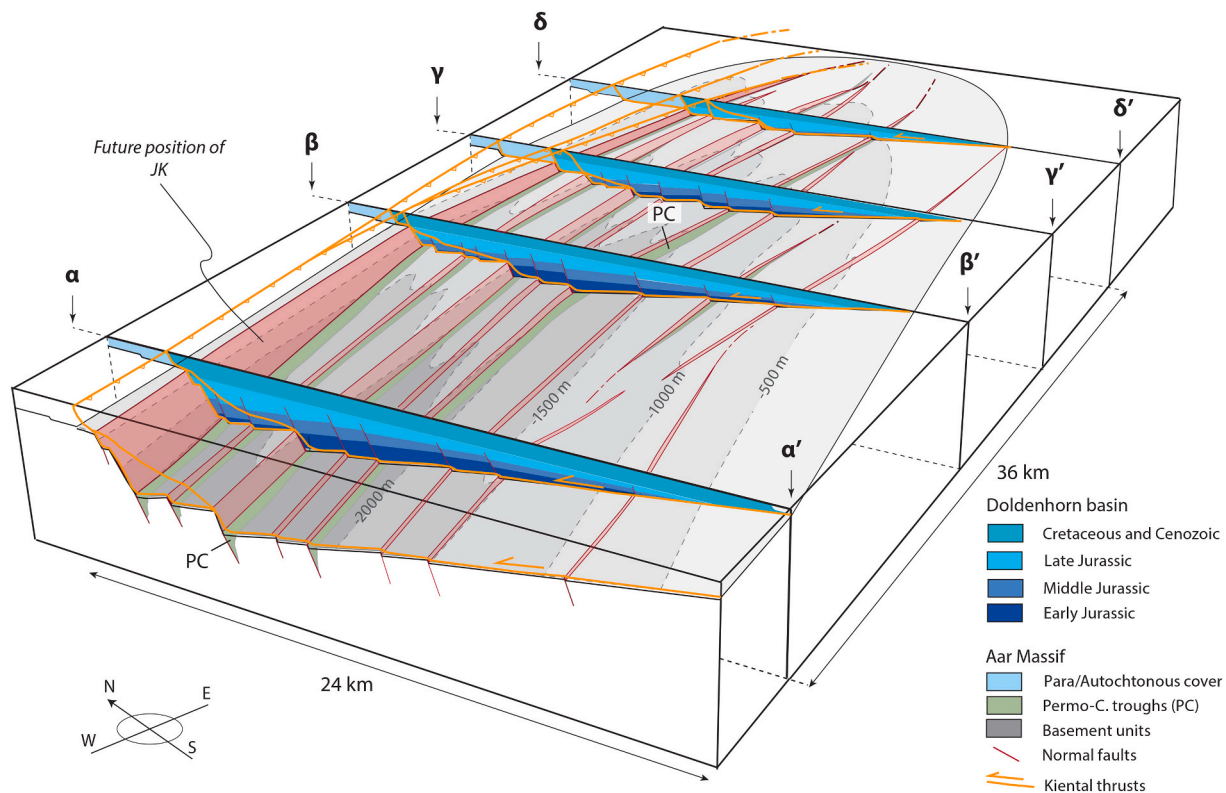


Fig. 10. 3D reconstruction of the shape of the Doldenhorn basin and relative sediment distribution. A series of Jurassic normal faults open an asymmetric half-graben, which is >2000 m deep in the West and <500 m deep in the East. The major Jurassic normal faults are often localized in Permo-Carboniferous half-graben (PC, green). The distribution of the sedimentary units within the basin reflects the asymmetric shape of the basin: (i) lower and middle Jurassic units respectively disappear and taper off in the eastern regions of the basin, whereas (ii) Upper Jurassic and Cretaceous and Cenozoic are reduced in thickness. Furthermore, the distribution of the Kiental basal thrusts (orange lines) evolves from a single basal thrust in the west to an in sequence series of thrusts in the East. (For interpretation of the references to colour in this figure legend, the reader is referred to the web version of this article.)

sedimentation is mainly restrained to the stretching basins (e.g. [Tugend et al., 2015](#); [Péron-Pinvidic et al., 2017](#); [Lymer et al., 2019](#)). This fact is corroborated, in case of the Doldenhorn Basin, by its long-lasting syn-rift sedimentation ranging from Early Jurassic until Cretaceous/Cenozoic times. Similar styles of sedimentation within asymmetric half-graben basins have been investigated in several recent large-scale examples such as the Jeanne d'Arc basin ([Welsink and Tankard, 2012](#); Newfoundland) or the Peniche basin ([Alves et al., 2006](#); Iberian margin).

Finally, we suggest that the asymmetric geometry of the Doldenhorn Basin relates directly to the reactivation of pre-existing crustal structures within the underlying basement units (e.g. [Santantonio and Carminati, 2011](#); [Lafosse et al., 2016](#); [Balázs et al., 2017](#)). Such reactivations, for example, have been previously inferred for the case of the Bourg d'Oisans ([Dumont et al., 2008](#)) or for the Pannonian and Aegean basins ([Balázs et al., 2017](#)). In the case of the Doldenhorn Basin, our 3D basin reconstruction indicates that the frequent occurrence of the major Mesozoic normal faults correlates directly with Permo-Carboniferous troughs. Hence, we interpret that the geometry of the Doldenhorn Basin and more generally of the European proximal continental margin was controlled by localization of normal faults within pre-existing Late Carboniferous-Permian crustal structures (e.g. see also [Badertscher and Burkhard, 1998](#); [Masini et al., 2013](#); [Balleuvre et al., 2018](#)).

5.2. Incipient thin-skinned dominated inversion of the Doldenhorn Basin

At 30 Ma, the thick wedge of Penninics, Austroalpine, and detached Helvetic nappes lying on top of the Doldenhorn Basin (Figs. 7a and 8a) was moving towards the north and triggered deformation in the Doldenhorn units. The overthrusting of the wedge led to strain localization in the Doldenhorn units and more specifically at the contact between the

basement and the sedimentary units. Indeed, the mechanically weak shale or anhydrite-rich layers of the Early Jurassic and Triassic units at the basement-cover transition provided an abrupt change in mechanical strength (e.g. [Pfiffner, 1993](#); [Bauville and Schmalholz, 2015](#)). The strain localization, which started at ~30 Ma in the Doldenhorn Basin, was therefore controlled by the initial geometry of the basin in combination with variation in mechanical strength of the involved basement and sedimentary units (Fig. 11). Consequently, not only rheological differences but also the variable along-strike top-basement topography and the resulting stratigraphic architecture controlled the deformation style. While a single basal thrust developed in the wider and deeper western region of the basin, the opposite occurred in the eastern regions where the thrust splayed into an in-sequence set of multiple imbricates (Fig. 10) consisting both of sediment and basement slices (see [Mair et al., 2018](#)). We explain this along-strike change in the development of the basal thrust system by the lateral variation of both the topography of the basement-cover interface as well as the thickness of the sedimentary units. These inferences correlate well with observations from 3D numerical studies (e.g. [Pfiffner, 1993](#); [Jammes and Huismans, 2012](#); [Nilfouroushan et al., 2013](#); [Bauville and Schmalholz, 2015](#)). At ~30 Ma, the sedimentary units of Doldenhorn Basin started to be detached from the basement units, which were then displaced towards the north along the newly developed basal shear zones. Because of the E-W trends in the rheological conditions, thin-skinned inversion tectonics (Kiental phase, Table 1) of the thicker sedimentary portion of the western part of the half-graben, resulted in the large-amplitude recumbent isoclinal fold with an intensively sheared thin overturned limb during progressive shearing and shortening (Figs. 7b and 11b). On the contrary, in the east, the Doldenhorn Nappe originated from the thinner portion of the half-graben, displayed only a small-amplitude fold (Figs. 8b and 11b) and

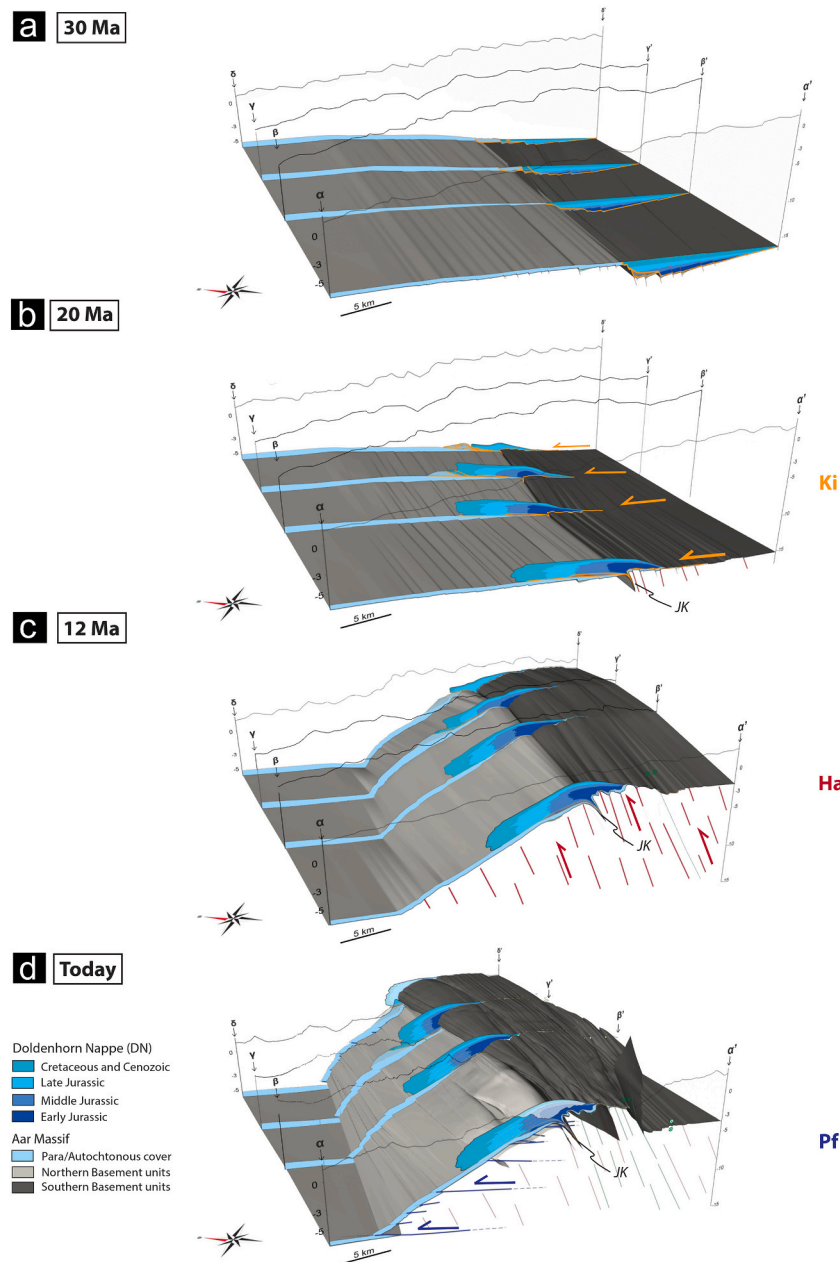


Fig. 11. 4D Reconstruction of the evolution of the Doldenhorn Basin (DN) and basement units. (A) Position of the DN basin on the European continental passive margin; (B) Thin-skinned thrusting of the sedimentary units driven by the Kiental thrusts; (C) Exhumation of the basement units induced by the Handegg structures and passive bulging of the overlying DN; (D) Current structural disposition of DN.

a sequence of autochthonous sediments as well as basement slivers (see Mair et al., 2018). As supported also by 3D numerical simulations (von Tscherner et al., 2016; Spitz et al., 2020), the non-cylindrical shape of the Doldenhorn Nappe (lateral variations in thickness and length of the resulting nappe; compare Figs. 6 and 10) is therefore a direct consequence of the former basin geometry. Furthermore, structural and 3D analogue studies (e.g. Thomas, 1977; Boyer and Elliott, 1982; Marshak et al., 1992; Macedo and Marshak, 1999; Mouthereau et al., 2002; Lacombe et al., 2003) of several salients of fold-and-thrust belts indicate that the initial large-scale basin architecture and sediment thickness variations strongly affect the development in fold-and thrust-belt salient. In addition, as discussed by Macedo and Marshak (1999) basin-controlled salients result in trend lines that converge at the end of the basin, and this finding is in accordance with the arcuate shape observed for the Doldenhorn thrust front (Fig. 11b, see also Doldenhorn Nappe

map 20 Ma, in Appendix B).

5.3. Exhumation of the basement units by thick-skinned deformation

At ~22 Ma, the onset of steep basement internal reverse faulting evolved with progressive shortening (onset of Handegg phase, Table 1), leading to a gradual differential uplift from south to north of the basement units. At this stage, strain localization in the basement units led to the generation of several steeply south-dipping brittle-ductile reverse faults and shear zones (see paragraph 5.5 and Herwegh et al., 2017). At the footwall of weakly reactivated normal faults, Triassic, Early and Middle Jurassic, and Permo-Carboniferous sediments were locally pinched in synformal sediment wedges, where the strata were steeply dipping and locally overturned (e.g. Bellahsen et al., 2012, 2014; Nibourel et al., 2021a; see appendix A for more information). The large-

scale manifestation of such inversion processes occurred at the border normal fault of the basin (Figs. 10 and 11). At this location, a sediment wedge was pinched between the basement units resulting in the presently exposed 'Jungfrau Keil'. This sediment wedge prominently separates the southern basement units from the northern ones (Fig. 11) and is continuous along the strike of the nappe from the West to the East (Fig. 1). The border of the basin consisted of a rotational normal fault with a larger throw in the West and a smaller one in the East (Fig. 10). Therefore, in the West the 'Jungfrau Keil' forms a > 2 km-deep wedge below the surface, which, in the East on the contrary, it only reaches a few hundred meters of depth. In terms of temperature-associated ductile deformation, the trace line of the basement-cover contact (Figs. 7c and 8c, see basement-cover contact trace), particularly in the case of the aforementioned sediment wedges, motivated a variety of studies to infer 'basement folding' as major deformation process (e.g. Heim, 1922; Ramsay et al., 1983; Ford, 1996; Krayenbuhl and Steck, 2009). However, peak metamorphic temperatures were too low (<400°C; Herwegh and Pfiffner, 2005; Berger et al., 2020; Girault et al., 2020) to allow for a pervasive ductile deformation of the granitoid basement units required to induce pervasive basement folds (see also Bellahsen et al., 2012; Lacombe and Bellahsen, 2016; and Appendix A for more information). Consequently, a network of steep Handegg shear zones dominated by viscous granular flow of fine-grained quartz-feldspar polymineralic mixtures (Wehrens et al., 2016) accommodated the reverse faulting and a vertical shearing. These movements together with erosion led to differential rock uplift. In contrast, shale rich and calcareous sediment units of the autochthonous and para-autochthonous cover as well as of the overlying sediment nappes were mechanically soft enough to accommodate strain in a fully ductile manner.

5.4. A switch back to thick-skinned dominated late-stage horizontal shortening

At 12 Ma, the tectonic style of deformation evolved to a thick-skinned horizontal tectonics stage. Indeed, flat to moderately SE dipping thrust zones with a NW-directed sense of shear initiated at the northern rim of the basement units of the Aar massif, cutting through all the above-mentioned structures and the basement-cover contact. Such discrete lower greenschist facies structures (Pfaffenchof thrusts; Table 1) led to thrusting of rigid slabs of southern basement over the northern basement units and wedging into the core of the mechanically weaker Doldenhorn Nappe units (Figs. 7, 8 and 11d). With progressive shortening, the thrust-domains progressed into a deeper crustal level, gradually steepening the basement-cover contact (Figs. 7, 8, and 11d) and leading to an en-bloc exhumation of the basement units (Herwegh et al., 2020; Nibourel et al., 2021a). It is due to this final thick-skinned horizontal tectonics stage that the impressive steep north walls of the Eiger, Mönch, Jungfrau, and Doldenhorn mountains were emplaced (see also Heim, 1922; Mair et al., 2018).

5.5. Implications for the inversion of a passive continental margin

The tectonic evolution of the Doldenhorn Nappe and Aar/Gastern Massifs exemplifies the large impact that basement involvement into the inversion of a proximal passive margin during a late-stage collision can have (see also Lacombe and Mouthereau, 2002; Lacombe and Bellahsen, 2016). Early stages of tectonic inversion of the proximal and distal parts of the former European passive continental margin were dominated by thin-skinned nappe tectonics (Pfiffner et al., 2011; Pfiffner, 2015). However, already at this stage, a major change in deformation occurred. Indeed, the thrusting-associated recumbent folding observed in the Doldenhorn and Morcles Nappes (lower Helvetic) clearly contrasts with the deformation characteristics of the already emplaced upper Helvetic nappes (e.g. Pfiffner, 1993; Escher et al., 1993; Escher and Beaumont, 1997; Pfiffner et al., 2011; Spitz et al., 2020), where thrusting, imbrication and open to narrow upright folding dominated. The variation in

deformation style between upper and lower Helvetic nappes resulted from the relatively high temperatures during deformation of the latter (275 to 380 °C; Herwegh and Pfiffner, 2005; Leloup et al., 2005; Boutoux et al., 2016; Berger et al., 2020; Girault et al., 2020, 2022). This temperature increase allowed shales and calcareous sediments to respond by a pervasive ductile deformation, in contrast with the colder temperatures of deformation during emplacement of the upper Helvetic nappes. With progressive shortening, subsequent thick-skinned nappe tectonics was initiated. This deformation stage (Handegg phase; Table 1) has been interpreted to be induced by buoyancy forces imposing on mid/upper crustal rocks, which had been decoupled from underlying European lower crust and lithospheric mantle (Herwegh et al., 2017; Kissling and Schlunegger, 2018). Finally, the late-stage horizontal thick-skinned deformation of the Aar Massif basement units (Pfaffenchof phase; Table 1) is inferred to be kinematically linked to deformation in the Alpine foreland. This deformation phase triggered imbricate thrusting of the Subalpine Molasse (von Hagke et al., 2012, 2014; Mock et al., 2020) as well as thrusting of the Jura along a basal detachment (e.g. Burkhard and Sommaruga, 1998; Sommaruga et al., 2012) or within the basement units (e.g. Becker, 2000; Lacombe and Mouthereau, 2002; Ustaszewski and Schmid, 2006, 2007; Madritsch et al., 2008; Lacombe and Bellahsen, 2016).

From ~22 Ma onwards, the ~12 to 17.5 km horizontal shortening and the 18 to 20 km maximum vertical uplift induced by basement tectonics (Fig. 9) had a dramatic impact on the Doldenhorn Nappe, forming the structural configuration presently observable. As discussed by Lacombe and Bellahsen (2016), most of the fold-and-thrust belts on Earth, even the 'classic' thin-skinned belts, show evidence of basement-involved shortening (e.g. Taiwan, Zagros). Thus assessing the degree of involvement of basement tectonics is crucial both for understanding the past kinematic evolution of a fold-and-thrust belt, and for predicting their short and long-term potential evolution. For instance, in the Taiwan fold-and-thrust belt the characterization of the degree of crustal coupling within the belt has been essential to identify faulting sources in the process of seismic hazard estimation (Camanni et al., 2014). However, the same concepts are applicable for assessing the potential of natural resources such as geothermal energy (Younas et al., 2016) or for selecting potential reservoirs for CO₂ sequestration (e.g. Chevalier et al., 2010).

6. Conclusion

A 4D reconstruction allowed us to quantitatively describe the structural evolution of the Doldenhorn Nappe and Aar/Gastern Massifs during the late-stage Alpine collision. The remarkable along-strike variability of the Doldenhorn Nappe and nearby Aar/Gastern Massifs basement units is the result of multiple preconditioning factors and deformation phases that shaped this tectonic complex through space and time. In particular these are:

- i) The Doldenhorn Nappe is the result of the inversion of a basement-cover system originally located along the proximal part of the European continental passive margin. The Doldenhorn Basin was located within an asymmetric half-graben bound by rotational normal faults. The non-cylindrical extension of the Doldenhorn Basin in the N-S and E-W directions resulted from the reactivation of pre-existing crustal fault structures within the basement units. The asymmetric shape of the half-graben affected the nature of the *syn*-tectonic sedimentary units within the basin, generating fluctuations in thickness along the strike of the basin and thickening towards the footwalls of the extensional faults.
- ii) During the incipient thin-skin-dominated inversion of the Doldenhorn Basin, strain localization occurred within the mechanically weak sedimentary units at the basement-cover transition (e.g. within shale-rich and evaporitic layers). Due to the varying topography of the basement-cover interface and thickness of the

sedimentary units, the resulting detachment horizon was localized along a single basal thrust in the west, while being split into an in-sequence set of thrusts in the eastern regions of the basin, also incorporating basement slivers. The aforementioned variations in incipient basin sediment thicknesses correlate directly with along-strike amplitude variation of the extruded Doldenhorn Nappe (large amplitude in the West; small amplitude in the East).

- iii) The multiphase thick-skinned deformation that overprinted the Doldenhorn Nappe from 22 Ma until present dramatically changed the shape of the investigated area, with a differential vertical exhumation followed by sub-horizontal thrusting of the basement units. The progressive sequence of these deformation phases led (i) to an overall updoming of both the Aar/Gastern Massifs and the entire Helvetic/Penninic/Austroalpine nappe stack on top, as well as (ii) to N-directed thrusting of rigid basement into the core of the Doldenhorn Nappe units.

The 4D reconstruction of the Doldenhorn Nappe and Aar/Gastern Massifs allows visualization of the 3D morphology and variability of a portion of the former proximal passive continental margin, of which current corresponding examples can be found along the Newfoundland or Iberian passive continental margins. The reconstructed subsequent inversion of the Doldenhorn Nappe and Aar/Gastern Massifs, as well as its along-strike variability by inheritance of pre-existing basin geometric and fault patterns, correlate well with recent analogue and numerical modelling studies. Our reconstruction illustrates how thin-skinned nappe formation mechanisms and the nappe geometries are controlled by the initial basement geometry and by the rheological strength contrasts between basement and cover sediments, while basement-involved uplift and shortening controls the late-stage collisional overprint and mechanics of the fold-and-thrust belts.

Author contributions

MH, AB, RB, and AM acquired the findings for this project. FMP, MH, DM and AB designed the study; whereas FMP, MH and DM carried out the fieldwork. FMP carried out the retrodeformation and modelling with additional scientific input from MH, AB, DM and technical assistance provided from MW and EK. FMP prepared the manuscript and figures with contribution from all co-authors. All authors read and approved the final manuscript.

Declaration of Competing Interest

The authors declare that they have no known competing financial interests or personal relationships that could have appeared to influence the work reported in this paper.

Data availability

Data will be made available on request.

Acknowledgments

We acknowledge Petroleum Experts (Petex) for providing an academic version of Move™, licensed to the Institute of Geological Sciences of the University of Bern. Our study was supported by the Federal Office of Topography of Switzerland (swisstopo; 570 300 4426 ARIWA 9101-01-Vertraege). We gratefully acknowledge Geotest AG for joint collaboration in the field, in particular H. Hartung-Hofmann, Sacha Wettstein and T. Wicki. S. Truttmann is thanked for helpful discussions, R. Tamblin for kindly proofreading the manuscript. The three reviewers (one anonymous, O. Lacombe and L. Cardello) together with the Editor S. Angiboust, are acknowledged for helpful advice that significantly improved the manuscript.

Appendix. Supplementary data

Supplementary data to this article can be found online at <https://doi.org/10.1016/j.tecto.2022.229586>.

References

- Abrecht, J., 1994. Geologic units of the Aar massif and their pre-Alpine rock associations: a critical review: the pre-Alpine crustal evolution of the Aar-, Gotthard-and Tavetsch massifs. *Schweiz. Mineral. Petrogr. Mitt.* 74 (1), 5–27.
- Allmendinger, R.W., Jordan, T.E., Kay, S.M., Isacks, B.L., 1997. The evolution of the Altiplano-Puna plateau of the Central Andes. *Annu. Rev. Earth Planet. Sci.* 25, 139–174.
- Alves, T.M., Moita, C., Sandnes, F., Cunha, T., Monteiro, J.H., Pinheiro, L.M., 2006. Mesozoic-Cenozoic evolution of North Atlantic continental-slope basins: the Peniche basin, western Iberian margin. *AAPG Bull.* 90, 31–60.
- Arkai, P., Ferreiro-Mählmann, R., Suchy, V., Balogh, K., Sykorova, I., Frey, M., 2002. Possible effects of tectonic shear strain on phyllosilicates: a case study from the Kandersteg area, Helvetic domain, Central Alps, Switzerland. *Schweiz. Mineral. Petrogr. Mitt.* 82, 273–290.
- Badertscher, N., Burkhard, M., 1998. Inversion alpine du graben Permo-Carbonifère de Salvan-Dorénez et sa relation avec le chevauchement de la nappe de Morcles sus-jacente. *Eclogae Geol. Helv.* 91, 359–373.
- Balázs, A., Matenco, L., Magyar, I., Horváth, F., Cloetingh, S., 2016. The link between tectonics and sedimentation in back-arc basins: new genetic constraints from the analysis of the Pannonian Basin. *Tectonics* 35 (6), 1526–1559.
- Balázs, A., Burrov, E., Matenco, L., Vogt, K., Francois, T., Cloetingh, S., 2017. Symmetry during the syn- and post-rift evolution of extensional back-arc basins: the role of inherited orogenic structures. *Earth Planet. Sci. Lett.* 462, 86–98.
- Balestra, M., Corrado, S., Aldega, L., Rudkiewicz, J.L., Morticelli, M.G., Sulli, A., Sassi, W., 2019. 3D structural modeling and restoration of the Apennine-Maghrebain chain in Sicily: application for non-cylindrical fold-and-thrust belts. *Tectonophysics* 761, 86–107.
- Balleve, M., Manzotti, P., Dal Piaz, G.V., 2018. Pre-Alpine (Variscan) inheritance: a key for the location of the future Valais Basin (Western Alps). *Tectonics* 37 (3), 786–817.
- Bally, A.W., Gordy, P., Stewart, G.A., 1966. Structure, seismic data, and orogenic evolution of southern Canadian Rocky Mountains. *Bull. Can. Petrol. Geol.* 14 (3), 337–381.
- Baumberger, R., Herwegh, M., Kissling, E., 2022. Remote sensing and field data based structural 3D modelling (Haslital, Switzerland) in combination with uncertainty estimation and verification by underground data. In: *3D Digital Geological Models: From Terrestrial Outcrops to Planetary Surfaces*, pp. 159–197.
- Bauville, A., Schmalholz, S.M., 2015. Transition from thin- to thick-skinned tectonics and consequences for nappe formation: numerical simulations and applications to the Helvetic nappe system, Switzerland. *Tectonophysics* 665, 101–117.
- Bauville, A., Schmalholz, S.M., 2017. Tectonic inheritance and kinematic strain localization as trigger for the formation of the Helvetic nappes, Switzerland. *Swiss J. Geosci.* 110 (2), 523–534.
- Becker, A., 2000. The Jura Mountains—an active foreland fold-and-thrust belt? *Tectonophysics* 321, 381–406.
- Bellahsen, N., Jolivet, L., Lacombe, O., Bellanger, M., Boutoux, A., Garcia, S., Mouthereau, F., Le Pourhiet, L., Gumiaux, C., 2012. Mechanisms of margin inversion in the external Western Alps: implications for crustal rheology. *Tectonophysics* 560, 62–83.
- Bellahsen, N., Mouthereau, F., Boutoux, A., Bellanger, M., Lacombe, O., Jolivet, L., Rolland, Y., 2014. Collision kinematics in the western external Alps. *Tectonics* 33 (6), 1055–1088.
- Berger, A., Wehrens, P., Lanari, P., Zwingmann, H., Herwegh, M., 2017. Microstructures, mineral chemistry and geochronology of white micas along a retrograde evolution: an example from the Aar massif (Central Alps, Switzerland). *Tectonophysics* 721, 179–195.
- Berger, A., Engi, M., Erne-Schmid, S., Glotzbach, C., Spiegel, C., de Goede, R., Herwegh, M., 2020. The relation between peak metamorphic temperatures and subsequent cooling during continent–continent collision (western Central Alps, Switzerland). *Swiss J. Geosci.* 113 (1), 1–18.
- Bigi, S., Carminati, E., Aldega, L., Trippetta, F., Kavoosi, M.A., 2018. Zagros fold and thrust belt in the Fars province (Iran): control of thickness/rheology of sediments and pre-thrusting tectonics on structural style and shortening. *Mar. Pet. Geol.* 91, 211–224.
- Boutoux, A., Bellahsen, N., Lacombe, O., Verlaquet, A., Mouthereau, F., 2014. Inversion of pre-orogenic extensional basins in the external Western Alps: structure, microstructures and restoration. *J. Struct. Geol.* 60, 13–29.
- Boutoux, A., Bellahsen, N., Nanni, U., Pik, R., Verlaquet, A., Rolland, Y., Lacombe, O., 2016. Thermal and structural evolution of the external Western Alps: Insights from (U–Th–Sm)/He thermochronology and RSCM thermometry in the Aiguilles Rouges/Mont Blanc massifs. *Tectonophysics* 683, 109–123.
- Boyer, S.E., Elliott, D., 1982. Thrust systems. *AAPG Bull.* 66 (9), 1196–1230.
- Burkhard, M., 1988. L'Helvétique de la bordure occidentale du massif de l'Aar (évolution tectonique et métamorphique). *Eclogae Geol. Helv.* 81 (1), 63–114.
- Burkhard, M., Sommaruga, A., 1998. Evolution of the western Swiss Molasse basin: structural relations with the Alps and the Jura belt. *Geol. Soc. Lond., Spec. Publ.* 134, 279–298.

- Butler, R.W., Tavarnelli, E., Grasso, M., 2006. Structural inheritance in mountain belts: an Alpine–Apennine perspective. *J. Struct. Geol.* 28 (11), 1893–1908.
- Camanni, G., Chen, C., Brown, D., Alvarez-Marron, J., Wu, Y., Chen, H., Huang, H., Chu, H., Chen, M., Chang, C., 2014. Basin inversion in central Taiwan and its importance for seismic hazard. *Geology* 42 (2), 147–150. <https://doi.org/10.1130/G35102.1>.
- Campani, M., Mulch, A., Kempf, O., Schlunegger, F., Mancktelow, N., 2012. Miocene paleotopography of the Central Alps. *Earth Planet. Sci. Lett.* 337, 174–185.
- Campani, M., Mancktelow, N., Courrioux, G., 2014. The 3D interplay between folding and faulting in a syn-orogenic extensional system: the Simplon Fault Zone in the Central Alps (Switzerland and Italy). *Swiss J. Geosci.* 107 (2), 251–271.
- Cardello, G.L., Di Vincenzo, G., Giorgetti, G., Zwingmann, H., Mancktelow, N., 2019. Initiation and development of the Pennine Basal Thrust (Swiss Alps): a structural and geochronological study of an exhumed megathrust. *J. Struct. Geol.* 126, 338–356.
- Cardello, G.L., Mancktelow, N., 2014. Cretaceous syn-sedimentary faulting in the Wildhorn Nappe. *Swiss J. Geosci.* 107 (2–3), 223–250. <https://doi.org/10.1007/s00015-014-0166-8>.
- Cardello, G.L., Mancktelow, N., 2015. Veining and post-nappe transtensional faulting in the SW Helvetic Alps (Switzerland). *Swiss J. Geosci.* 108 (2–3), 1–22. <https://doi.org/10.1007/s00015-015-0199-7>.
- Cardello, G.L., Almqvist, B.S., Hirt, A.M., Mancktelow, N.S., 2016a. Determining the timing of formation of the Rawil Depression in the Helvetic Alps by palaeomagnetic and structural methods. *Geol. Soc. Lond., Spec. Publ.* 425 (1), 145–168.
- Cardello, G.L., Almqvist, B.S., Hirt, A.M., Mancktelow, N.S., 2016b. Determining the timing of formation of the Rawil Depression in the Helvetic Alps by palaeomagnetic and structural methods. *Geol. Soc. Lond., Spec. Publ.* 425 (1), 145–168.
- Chamberlin, R.T., 1919. The building of the Colorado Rockies. *J. Geol.* 27 (4), 225–251.
- Chevalier, G., Diamond, L.W., Leu, W., 2010. Potential for deep geological sequestration of CO₂ in Switzerland: a first appraisal. *Swiss J. Geosci.* 103 (3), 427–455.
- Cooper, M., 2007. Structural style and hydrocarbon prospectivity in fold and thrust belts: a global review. In: *Special Publication-Geological Society of London*, 272, p. 447.
- Curzi, M., Aldega, L., Bernasconi, S.M., Berra, F., Billi, A., Boschi, C., Franchini, S., Van der Lelij, R., Viola, G., Carminati, E., 2020. Architecture and evolution of an extensionally-inverted thrust (Mt. Tancia Thrust, Central Apennines): geological, structural, geochemical, and K–Ar geochronological constraints. *J. Struct. Geol.* 136, 104059.
- Doglionni, C., 1992. Relationships between Mesozoic extensional tectonics, stratigraphy and Alpine inversion in the Southern Alps. *Eclogae Geol. Helv.* 85 (1), 105–126.
- Dollfuss, S., 1965. Über den helvetischen Dogger zwischen Linth und Rhein. *Eclogae Geol. Helv.* 58 (1), 453–554.
- Dumont, T., Champagnac, J.D., Crouzet, C., Rochat, P., 2008. Multistage shortening in the Dauphiné zone (French Alps): the record of Alpine collision and implications for pre-Alpine restoration. *Swiss J. Geosci.* 101 (1), 89–110.
- Ebert, A., Herwegh, M., Berger, A., Pfiffner, A., 2008. Grain coarsening maps for polymineralic carbonate mylonites: a calibration based on data from different Helvetic nappes (Switzerland). *Tectonophysics* 457, 128–142.
- Epard, J.L., 1990. La nappe de Morcles au sud-ouest du Mont-Blanc, PhD thesis. *Mém. Géol. Lausanne* 8, 1–158.
- Escher, A., Beaumont, C., 1997. Formation, burial and exhumation of basement nappes at crustal scale: a geometric model based on the Western Swiss-Italian Alps. *J. Struct. Geol.* 19, 955–974.
- Escher, A., Masson, H., Steck, A., 1993. Nappe geometry in the western Swiss Alps. *J. Struct. Geol.* 15, 501–509.
- Fitz-Diaz, E., Hudleston, P., Tolson, G., 2011. Comparison of tectonic styles in the Mexican and Canadian Rocky Mountain fold-thrust belt. *Geol. Soc. Lond., Spec. Publ.* 349 (1), 149–167.
- Ford, M., 1996. Kinematics and geometry of early Alpine, basement-involved folds, SW Pelvoux Massif, SE France. *Eclogae Geol. Helv.* 89, 269–295.
- Frey, M., 1987. The reaction-isograd kaolinite+quartz=pyrophyllite+H₂O, Helvetic Alps, Switzerland. *Schweiz. Mineral. Petrogr. Mitt.* 67, 1–11.
- Frey, M., Teichmueller, M., Teichmueller, R., Mullis, J., Kuenzi, B., Breitschmid, A., Gruner, U., Schwizer, B., 1980. Very low grade metamorphism in external parts of the Central Alps: illite crystallinity, coal rank and fluid inclusion data. *Eclogae Geol. Helv.* 73 (1), 173–203.
- Ghani, H., Zeilinger, G., Sobel, E.R., Heidarzadeh, G., 2018. Structural variation within the Himalayan fold and thrust belt: a case study from the Kohat-Potwar Fold Thrust Belt of Pakistan. *J. Struct. Geol.* 116, 34–46.
- Gillcrist, R., Coward, M., Mugnier, J.-L., 1987. Structural inversion and its controls: examples from the Alpine foreland and the French Alps. *Geodin. Acta* 1 (1), 5–34.
- Girault, J.B., Bellahsen, N., Boutoux, A., Rosenberg, C., Nanni, U., Verlaquet, A., Beyssac, O., 2020. 3D thermal structure of the Helvetic nappes of the European Alps: implications for collisional processes. *Tectonics*. <https://doi.org/10.1029/2018tc005334>.
- Girault, J.B., Bellahsen, N., Bernet, M., Pik, R., Loget, N., Lasseur, E., Rosenberg, C.L., Balvay, M., Sonnet, M., 2022. Exhumation of the Western Alpine collisional wedge: new thermochronological data. *Tectonophysics* 822, 229155.
- Granado, P., Ruh, J.B., 2019. Numerical modelling of inversion tectonics in fold-and-thrust belts. *Tectonophysics* 763, 14–29.
- Grosjean, G., Sue, C., Burkhard, M., 2004. Late Neogene extension in the vicinity of the Simplon fault zone (Central Alps, Switzerland). *Eclogae Geol. Helv.* 97 (1), 33–46.
- Hamilton, W.B., 1988. Laramide crustal shortening. In: *Interaction of the Rocky Mountain Foreland and the Cordilleran Thrust Belt: Geological Society of America Memoir*, 171, pp. 27–39.
- Hänni, R., Pfiffner, O.A., 2001. Evolution and internal structure of the Helvetic nappes in the Bernese Oberland. *Eclogae Geol. Helv.* 94 (2), 161–171.
- Heim, A., 1922. *Geologie der Schweiz*, 2. CH Tauchnitz.
- Herwegh, M., Pfiffner, O.-A., 2005. Tectono-metamorphic evolution of a nappe stack: a case study of the Swiss Alps. *Tectonophysics* 404 (1–2), 55–76.
- Herwegh, M., Berger, A., Baumberger, R., Wehrens, P., Kissling, E., 2017. Large-scale crustal-block-extrusion during late Alpine collision. *Sci. Rep.* 7 (1), 1–10.
- Herwegh, M., Berger, A., Glotzbach, C., Wangenheim, C., Mock, S., Wehrens, P., Baumberger, R., Egli, D., Kissling, E., 2020. Late stages of continent-continent collision: timing, kinematic evolution, and exhumation of the Northern rim (Aar Massif) of the Alps. *Earth Sci. Rev.* 200, 102959 <https://doi.org/10.1016/j.earscirev.2019.102959>.
- Huon, S., Burkhard, M., Hunziker, J.-C., 1994. Mineralogical, K–Ar, stable and Sr isotope systematics of K-white micas during very low-grade metamorphism of limestones (Helvetic nappes, western Switzerland). *Chem. Geol.* 113, 347–376.
- Jammes, S., Huisman, R.S., 2012. Structural styles of mountain building: controls of lithospheric rheologic stratification and extensional inheritance. *J. Geophys. Res. Solid Earth* 117 (B10).
- Jaquet, Y., Duret, T., Grujic, D., Masson, H., Schmalholz, S.M., 2018. Formation of orogenic wedges and crustal shear zones by thermal softening, associated topographic evolution and application to natural orogens. *Tectonophysics* 746, 512–529.
- Kempf, O., Pfiffner, O.A., 2004. Early Tertiary evolution of the North Alpine Foreland Basin of the Swiss Alps and adjoining areas. *Basin Res.* 16 (4), 549–567.
- Kissling, E., Schlunegger, F., 2018. Rollback orogeny model for the evolution of the Swiss Alps. *Tectonics* 37, 1097–1115.
- Krayenbuhl, T., Steck, A., 2009. Structure and kinematics of the Jungfrau syncline, Fafertal (Valais, Alps), and its regional significance. *Swiss J. Geosci.* 102, 441–456. <https://doi.org/10.1007/s00015-009-1333-1>.
- Krebs, J., 1925. *Geologische Beschreibung der Blümlisalp-Gruppe Beiträge zur Geol. Karte der Schweiz*, N.F. 54. Francke, Bern.
- Lacombe, O., Bellahsen, N., 2016. Thick-skinned tectonics and basement-involved fold–thrust belts: insights from selected Cenozoic orogens. *Geol. Mag.* 153, 763–810.
- Lacombe, O., Mouthereau, F., 2002. Basement-involved shortening and deep detachment tectonics in forelands of orogens: insights from recent collision belts (Taiwan, Western Alps, Pyrenees). *Tectonics* 21 (4).
- Lacombe, O., Mouthereau, F., Angelier, J., Chu, H.T., Lee, J.C., 2003. Frontal belt curvature and oblique ramp development at an obliquely collided irregular margin: geometry and kinematics of the NW Taiwan fold-thrust belt. *Tectonics* 22 (3).
- Lafosse, M., Boutoux, A., Bellahsen, N., Le Pourhiet, L., 2016. Role of tectonic burial and temperature on the inversion of inherited extensional basins during collision. *Geol. Mag.* 153, 811–826.
- Leloup, P.-H., Arnaud, N., Sobel, E.R., Lacassin, R., 2005. Alpine thermal and structural evolution of the highest external crystalline massif: the Mont Blanc. *Tectonics* 24 (4).
- Letouzey, J., Werner, P., Marty, A., 1990. Fault reactivation and structural inversion. Backarc and intraplate compressive deformations. Example of the eastern Sunda shelf (Indonesia). *Tectonophysics* 183 (1–4), 341–362.
- Lymer, G., Cresswell, D.J., Reston, T.J., Bull, J.M., Sawyer, D.S., Morgan, J.K., Stevenson, C., Causar, A., Minshall, T.A., Shillington, D.J., 2019. 3D development of detachment faulting during continental breakup. *Earth Planet. Sci. Lett.* 515, 90–99.
- Macedo, J., Marshak, S., 1999. Controls on the geometry of fold-thrust belt salients. *Geol. Soc. Am. Bull.* 111 (12), 1808–1822.
- Madritsch, H., Schmid, S.M., Fabbri, O., 2008. Interactions between thin- and thick-skinned tectonics at the northwestern front of the Jura fold-and-thrust belt (eastern France). *Tectonics* 27 (5).
- Mair, D., Lechmann, A., Herwegh, M., Nibourel, L., Schlunegger, F., 2018. Linking Alpine deformation in the Aar Massif basement and its cover units—the case of the Jungfrau–Eiger mountains (Central Alps, Switzerland). *Solid Earth* 9, 1099–1122.
- Marshak, S., Wilkerson, M., Hsui, A., 1992. Generation of curved fold-thrust belts: insight from simple physical and analytical models. In: *Thrust Tectonics*. Springer, pp. 83–92.
- Masini, E., Manatschal, G., Mohn, G., 2013. The Alpine Tethys rifted margins: reconciling old and new ideas to understand the stratigraphic architecture of magma-poor rifted margins. *Sedimentology* 60 (1), 174–196.
- Masson, H., Herb, R., Steck, A., 1980. Helvetic Alps of Western Switzerland, excursion no. 1. In: Trümpy, R. (Ed.), *Geology of Switzerland – A Guide Book*, Part B, Geological Excursions. Wepf & Co, Basel, pp. 109–153.
- McClay, K.R., Whitehouse, P.S., Dooley, T., Richards, M., 2004. 3D evolution of fold and thrust belts formed by oblique convergence. *Mar. Pet. Geol.* 21 (7), 857–877.
- Mock, S., von Hagke, C., Schlunegger, F., Dunkl, I., Herwegh, M., 2020. Long-wavelength late-Miocene thrusting in the north Alpine foreland: implications for late orogenic processes. *Solid Earth* 11, 1823–1847.
- Mohn, G., Manatschal, G., Masini, E., Müntener, O., 2011. Rift-related inheritance in orogens: a case study from the Austroalpine nappes in Central Alps (SE-Switzerland and N-Italy). *Int. J. Earth Sci.* 100 (5), 937–961.
- Mohn, G., Manatschal, G., Beltrando, M., Haupt, I., 2014. The role of rift-inherited hyper-extension in Alpine-type orogens. *Terra Nova* 26 (5), 347–353.
- Mouthereau, F., Defontaine, B., Lacombe, O., Angelier, J., Byrne, T., Liu, C., 2002. Variations along the strike of the Taiwan thrust belt: basement control on structural style, wedge geometry, and kinematics. *Spec. Pap. Geol. Soc. Am.* 358, 35–58.
- Nemcok, M., Mora, A., Cosgrove, J., 2013. Thick-skin-dominated orogens; from initial inversion to full accretion: an introduction. *Geol. Soc. Lond., Spec. Publ.* 377, 1–17.
- Nibourel, L., Berger, A., Egli, D., Luensdorf, N.K., Herwegh, M., 2018. Large vertical displacements of a crystalline massif recorded by Raman thermometry. *Geology* 46 (10), 879–882.
- Nibourel, L., Rahn, M., Dunkl, I., Berger, A., Hermann, F., Diehl, T., Heuberger, S., Herwegh, M., 2021a. Orogen-parallel migration of exhumation in the eastern Aar Massif revealed by low-T thermochronometry. *J. Geophys. Res. Solid Earth* 126 e2020JB020799.

- Nibourel, L., Berger, A., Egli, D., Heuberger, S., Herwegh, M., 2021b. Structural and thermal evolution of the eastern Aar Massif: insights from structural field work and Raman thermometry. *Swiss J. Geosci.* 114 (1), 1–43.
- Nilfouroushan, F., Pysklywec, R., Cruden, A., Koyi, H., 2013. Thermal–mechanical modeling of salt-based mountain belts with pre-existing basement faults: application to the Zagros fold and thrust belt, Southwest Iran. *Tectonics* 32 (5), 1212–1226.
- Peron-Pinvidic, G., Manatschal, G., Osmundsen, P.T., 2013. Structural comparison of archetypal Atlantic rifted margins: a review of observations and concepts. *Mar. Pet. Geol.* 43, 21–47.
- Péron-Pinvidic, G., Manatschal, G., Masini, E., Sutra, E., Flament, J.M., Hauptert, I., Unternehr, P., 2017. Unravelling the along-strike variability of the Angola–Gabon rifted margin: a mapping approach. *Geol. Soc. Lond., Spec. Publ.* 438 (1), 49–76.
- Pfiffner, O.A., 1993. The structure of the Helvetic nappes and its relation to the mechanical stratigraphy. *J. Struct. Geol.* 15, 511–521.
- Pfiffner, O.A., 2006. Thick-skinned and thin-skinned styles of continental contraction. *Spec. Pap. Geol. Soc. Am.* 414, 153.
- Pfiffner, O.A., 2015. *Geologie der Alpen*, 8416. UTB.
- Pfiffner, O.A., Lehner, P., Heitzmann, P., Mueller, S., Steck, A., 1997. Deep structure of the Swiss Alps: results of NRP 20. *Birkhäuser* 1–380.
- Pfiffner, O.A., Burkhard, M., Hänni, R., Kammer, A., Kligfield, R., Mancktelow, N., Menkveld, J.W., Ramsay, J., Schmid, S.M., Zurbriegen, R., 2011. Structural Map of the Helvetic Zone of the Swiss Alps Geological Special Map 1:100'000. *Swisstopo*, Bern, p. 128.
- Ramsay, J., 1981. Tectonics of the Helvetic nappes. *Geol. Soc. Lond., Spec. Publ.* 9, 293–309.
- Ramsay, J.G., Casey, M., Kligfield, R., 1983. Role of shear in development of the Helvetic fold-thrust belt of Switzerland. *Geology* 11, 439–442.
- Rodgers, J., 1949. Evolution of thought on structure of middle and southern Appalachians. *AAPG Bull.* 33 (10), 1643–1654.
- Rohr, K., 1926. Stratigraphische und tektonische Untersuchung der Zwischenbildungen am Nordrand des Aarmassivs (zwischen Wendenjoch und Wetterhorn), Beiträge zur Geol. Karte der Schweiz, N.F. 57. Francke, Bern.
- Sala, P., Pfiffner, O.A., Frehner, M., 2014. The Alpstein in three dimensions: fold-and-thrust belt visualization in the Helvetic zone, eastern Switzerland. *Swiss J. Geosci.* 107 (2), 177–195.
- Santantonio, M., Carminati, E., 2011. Jurassic rifting evolution of the Apennines and Southern Alps (Italy): parallels and differences. *GSA Bull.* 123 (3–4), 468–484.
- Santolaria, P., Vendeville, B.C., Graveleau, F., Soto, R., Casas-Sainz, A., 2015. Double evaporitic décollements: influence of pinch-out overlapping in experimental thrust wedges. *J. Struct. Geol.* 76, 35–51.
- Schlunegger, F., Kissling, E., 2015. Slab rollback orogeny in the Alps and evolution of the Swiss Molasse basin. *Nat. Commun.* 6 (1), 1–10.
- Schmid, S.M., Fügenschuh, B., Kissling, E., Schuster, R., 2004. Tectonic map and overall architecture of the Alpine orogen. *Eclogae Geol. Helv.* 97, 93–117.
- Sommaruga, A., Eichenberger, U., Marillier, F.J.Y., 2012. Seismic Atlas of the Swiss Molasse Basin. In: *Swiss Geophysical Commission, Contribution to the Geology of Switzerland – Geophysics*, 44, pp. 1–82.
- Spitz, R., Bauville, A., Epard, J.L., Kaus, B.J., Popov, A.A., Schmalholz, S.M., 2020. Control of 3-D tectonic inheritance on fold-and-thrust belts: insights from 3-D numerical models and application to the Helvetic nappe system. *Solid Earth* 11 (3), 999–1026.
- Steck, A., 2008. Tectonics of the Simplon massif and Lepontine gneiss dome: deformation structures due to collision between the underthrusting European plate and the Adriatic indenter. *Swiss J. Geosci.* 101 (2), 515–546.
- Tavani, S., Cardello, G.L., Vignaroli, G., Balsamo, F., Parente, M., Sabbatino, M., Raffi, I., Billi, A., Carminati, E., 2021. Segmentation of the Apenninic margin of the Tyrrhenian Back-Arc Basin Forced by the Subduction of an Inherited Transform System. *Tectonics* 40 (9) e2021TC006770.
- Taylor, B., Goodliffe, A., Martinez, F., Hey, R., 1995. Continental rifting and initial sea-floor spreading in the Woodlark Basin. *Nature* 374 (6522), 534–537.
- Thomas, W.A., 1977. Evolution of Appalachian-Ouachita salients and recesses from reentrants and promontories in the continental margin. *Am. J. Sci.* 277, 1233–1278.
- Trümpy, R., 1952. Der Nordrand der Liasischen Tethys in den Schweizer Alpen. *Geol. Rundsch.* 40 (2), 239–242.
- Tugend, J., Manatschal, G., Kuznir, N.J., Masini, E., 2015. Characterizing and identifying structural domains at rifted continental margins: application to the Bay of Biscay margins and its Western Pyrenean fossil remnants. *Geol. Soc. Lond., Spec. Publ.* 413 (1), 171–203.
- Turrini, C., Lacombe, O., Roure, F., 2014. Present-day 3D structural model of the Po Valley basin, Northern Italy. *Mar. Pet. Geol.* 56, 266–289.
- Turrini, C., Toscani, G., Lacombe, O., Roure, F., 2016. Influence of structural inheritance on foreland-foredeep system evolution: an example from the Po valley region (northern Italy). *Mar. Pet. Geol.* 77, 376–398.
- Ustaszewski, K., Schmid, S.M., 2006. Control of preexisting faults on geometry and kinematics in the northernmost part of the Jura fold-and-thrust belt. *Tectonics* 25, TC5003.
- Ustaszewski, K., Schmid, S.M., 2007. Latest Pliocene to recent thick-skinned tectonics at the Upper Rhine Graben–Jura Mountains junction. *Swiss J. Geosci.* 100, 293–312.
- Vitale, S., Ciarcia, S., 2021. The dismembering of the Adria platforms following the late Cretaceous-Eocene abortive rift: a review of the tectono-stratigraphic record in the southern Apennines. *Int. Geol. Rev.* <https://doi.org/10.1080/00206814.2021.2004559>.
- von Hagke, C., Cederbom, C., Oncken, O., Stöckli, D., Rahn, M., Schlunegger, F., 2012. Linking the northern Alps with their foreland: the latest exhumation history resolved by low-temperature thermochronology. *Tectonics* 31, TC5010.
- von Hagke, C., Oncken, O., Evseev, S., 2014. Critical taper analysis reveals lithological control of variations in detachment strength: an analysis of the Alpine basal detachment (Swiss Alps). *Geochem. Geophys. Geosyst.* 15, 176–191.
- von Tscharner, M., Schmalholz, S., Epard, J.-L., 2016. 3-D numerical models of viscous flow applied to fold nappes and the Rawil depression in the Helvetic nappe system (western Switzerland). *J. Struct. Geol.* 86, 32–46.
- Watts, A., Lamb, S., Fairhead, J., Dewey, J., 1995. Lithospheric flexure and bending of the Central Andes. *Earth Planet. Sci. Lett.* 134, 9–21.
- Wehrens, P., Berger, A., Peters, M., Spillmann, T., Herwegh, M., 2016. Deformation at the frictional-viscous transition: evidence for cycles of fluid-assisted embrittlement and ductile deformation in the granitoid crust. *Tectonophysics* 693, 66–84.
- Wehrens, P., Baumberger, R., Berger, A., Herwegh, M., 2017. How is strain localized in a meta-granitoid, mid-crustal basement section? Spatial distribution of deformation in the central Aar massif (Switzerland). *J. Struct. Geol.* 94, 47–67.
- Welsink, H., Tankard, A., 2012. 14-Extensional tectonics and stratigraphy of the Mesozoic Jeanne d'Arc basin. In: *Grand Banks of Newfoundland, Regional Geology and Tectonics: Phanerozoic Rift Systems and Sedimentary Basins*, 1, p. 337.
- Wilson, R.C.L., Manatschal, G., Wise, S., 2001. Rifting along non-volcanic passive margins: stratigraphic and seismic evidence from the Mesozoic successions of the Alps and western Iberia. In: *Wilson, R.C.L., Whitmarsh, R.B., Taylor, B., Fritzsche, N. (Eds.), Non-volcanic Rifting of Continental Margins: A Comparison of Evidence from Land and Sea*. Geological Society, London, pp. 429–452.
- Younas, U., Khan, B., Ali, S.M., Arshad, C.M., Farid, U., Zeb, K., Rehman, F., Mehmood, Y., Vaccaro, A., 2016. Pakistan geothermal renewable energy potential for electric power generation: a survey. *Renew. Sust. Energ. Rev.* 63, 398–413.
- Zanchi, A., Berra, F., Mattei, M., Ghassemi, M.R., Sabouri, J., 2006. Inversion tectonics in central Alborz, Iran. *J. Struct. Geol.* 28 (11), 2023–2037.
- Ziegler, H.J., Isler, A., 2013. Zusammenfassender geologischer Schlussbericht Lötschberg-Basistunnel. *Landesgeologie (Bundesamt für Landestopografie swisstopo)*, Wabern, Switzerland.